Biomolecules and Biomedicine

ISSN: 2831-0896 (Print) | ISSN: 2831-090X (Online)

Journal Impact Factor® (2023): 3.1

CiteScore®(2023):7.4

www.biomolbiomed.com | www.blog.bjbms.org

RESEARCH ARTICLE

Zhang et al: Glioblastoma activates CAF-like astrocytes

Glioblastoma induces CAF-like astrocyte activation via the AKT/mTOR–SERPINH1/COL5A1 axis

Jingxian Zhang[2#], Yajia Chen[2#] and Hongwu Xu[1,2*]

[1]Neurosurgery Department, The Tenth Affiliated Hospital, Southern Medical University, Dongguan, Guangdong Province, China;

[2]Departmant of Human Anatomy,Shantou University Medical College, Jinping District, Shantou, Guangdong, China.

*Correspondence to **Hongwu Xu**: hwxu@smu.edu.cn

#**Jingxian Zhang** and **Yajia Chen** contributed equally to this work.

DOI: https://doi.org/10.17305/bb.2025.11898

ABSTRACT

Glioblastoma multiforme (GBM), the most aggressive form of glioma, remains the most malignant tumor of the central nervous system. Despite a range of therapeutic strategies, the prognosis for GBM patients remains poor, underscoring the urgent need for novel treatments to inhibit GBM progression. The tumor microenvironment (TME) plays a critical role in tumor development, with cancer-associated fibroblasts (CAFs) acting as key components. However, the origin, composition, and spatial distribution of CAFs within the GBM microenvironment remain poorly understood. To address this gap, our research aims to investigate the etiology, cellular composition, and precise localization of CAFs in GBM, with the goal of elucidating their role in oncogenesis and tumor progression, thereby providing new avenues for therapeutic intervention. In this study, we developed a novel CAF-related prognostic model using data from the TCGA and GEO databases and identified *SERPINH1* and *COL5A1* as CAF-related genes in GBM. We established a GBM mouse model as well as a GBM cell and astrocyte co-culture system to examine the expression of *SERPINH1* and *COL5A1* in astrocytes under a simulated tumor microenvironment. Our findings revealed that these genes were more highly expressed in peritumoral tissue compared to normal brain tissue and showed strong co-localization with astrocytes. Furthermore, we found that normal astrocytes can be induced by GBM cells to activate the AKT/mTOR signaling pathway, migrate to the peritumoral region, and upregulate CAF-associated proteins (SERPINH1/COL5A1). These results suggest that astrocytes may serve as a potential source of CAF precursor cells within the GBM tumor microenvironment.

Keywords: glioblastoma; cancer-associated fibroblasts; CAFs; astrocytes; SERPINH1; COL5A1; AKT/mTOR pathway.

INTRODUCTION

Glioblastoma multiforme (GBM), also known as glioblastoma or malignant glioma, accounts for approximately 57% of all gliomas and 48% of all primary malignant central nervous system (CNS) tumors(1). Despite recent advances in the treatment of glioblastoma, including surgical resection, radiotherapy, systemic therapies (chemotherapy, targeted therapy), and

supportive care, the overall prognosis remains poor, with low long-term survival rates. The median overall survival among patients with glioblastoma is approximately 12 to 18 months(2). GBM mainly originates from glial cells, and can also develop from neural stem cells(3). Temozolomide (TMZ) is a second-generation anti-cancer drug that can easily pass through the blood-brain barrier (BBB) and is currently used as a first-line chemotherapeutic agent against GBM. However, GBM can quickly become resistant to TMZ and can potentially relapse after TMZ-mediated treatment(4, 5). To find new therapeutic approaches, recent studies have been focused not only on the treatment of GBM, but also on the tumor microenvironment (TME).

The TME is made up of tumor cells, their surrounding immune cells, and the associated stromal components. The TME includes the extracellular matrix (ECM), stromal cells (such as fibroblasts and immune, inflammatory, endothelial, and bone marrow-derived cells), cytokines, and chemokines(6-9). The TME is associated with GBM resistance to targeted therapy(10), intra-tumor heterogeneity(11), and invasiveness(12). Therefore, studying the interactions between TME and GBM may lead to the discovery of new mechanisms related to the treatment of GBM.

Cancer-associated fibroblasts (CAFs) play essential roles as components of TME. These roles include deposition and remodeling of the extracellular matrix (ECM), immunomodulation, promotion of angiogenesis, facilitation of metabolic processes, and reprogramming of the TME(13-16). The origins of CAFs are diverse and include, but are not limited to, intrinsic fibroblasts, tumor epithelial and endothelial cells, and normal epithelial-tissue cells(16). CAFs show different degrees of heterogeneity and have different markers(16). Growing evidence indicates that CAFs are involved, and play important roles, in the development, progression, immunosuppression, and drug resistance of various cancers. Current research examining the roles of CAFs in tumorigenesis and treatment resistance has been focused on subgroup analyses and functional studies. These approaches rely on CAF-specific markers (FAP, α-SMA) and secretagogues (IFN-γ, TGF-β), which are expressed at different levels in a context-specific manner at different cancer stages(17, 18). In a recent study, Phillip et al. discovered, through single-cell sequencing and bioinformatics analysis, the presence of a limited population of CAFs within GBM. Despite their relative scarcity, these CAFs were found to play a crucial role in tumor grading and patient prognosis(19). Considering the significant role of CAFs in various tumors, their origin, composition, and precise localization within the microenvironment of GBM remain to be fully elucidated. Therefore, studying the

interaction between CAFs and GBM may lead to the development of new anti-GBM therapies.

To identify genes associated with CAFs that are uniquely expressed in GBM, we used the combined TCGA- and GEO-derived GBM datasets to construct a new CAF-related GBM prognostic model. Two CAF hub genes (SERPINH1 and COL5A1) expressed in GBM were screened using this model. These two genes were then confirmed as CAF markers for GBM using a CAF scoring correlation analysis. A GBM mouse model was constructed to verify the expression of SERPINH1 and COL5A1 in GBM. Our results obtained using this model show that protein expression levels of SERPINH1 and COL5A1 were high in the peritumor tissue relative to those in normal tissue. A co-localization assay performed using mouse brain tissue was used to explore the localization of SERPINH1 and COL5A1 in the peritumor tissue. We found that large aggregates of activated astrocytes around the tumor were highly correlated with increased protein expression levels of SERPINH1 and COL5A1. Results obtained using our in-vitro cell co-culture model showed that GBM cells could indeed recruit astrocytes to the periphery of the tumor, and activate and overexpress SERPINH1 and COL5A1. Results obtained using bioinformatics and western blotting showed that this activation may have occurred via the AKT/mTOR pathway. In conclusion, our results indicate that GBM exerted regulatory effects on peripheral cells (particularly astrocytes) via the AKT/mTOR-SERPINH1/COL5A1 axis, directing these astrocytes to become activated and play CAF-like roles. It is possible that these CAF-like cells are potentially involved in a wide range of pathological conditions.

MATERIALS AND METHODS

Data acquisition

Clinical information, and transcriptional and mutation data, for GBM were obtained using The Cancer Genome Atlas (TCGA; https://cancergenome.nih.gov/) and GEO (https://www.ncbi.nlm.nih.gov/geo/) databases. TCGA database contained 600 tumor samples with clinical characteristics including age, sex, survival status, survival time, and tumor grade IV. TCGA mutation data were also downloaded for subsequent analysis. The probe matrix (GSE43378) and platform (GPL570) files for the expression data obtained from patients with glioma, including age, sex, survival status, and survival time, were downloaded from the GEO dataset. TCGA and GEO data were annotated, and mRNA expression data

were differentiated, separately for subsequent analyses. The steps used in this procedure are shown in the following flowchart.

Fibroblast and TIDE scoring

Tumor immune dysfunction and exclusion (TIDE) (http://tide.dfci.harvard.edu/login/), designed by Jiang et al(20)., is a new computational framework used to predict the role of tumor immune escape mechanisms and resistance to immunotherapy. In our present study, this framework was used to obtain the tumor immune dysfunction and exclusion TIDE scoring file and fibroblast scoring file from TCGA and GEO. Perl was utilized to prepare the TIDE scoring file using average recurring mRNA expression. We then removed the normal samples and took the logarithm of the mRNA expression value. Fibroblast scoring was performed using the R packages "EPIC," "MCPcounter," and "xCell"(21). Model construction and subsequent bioinformatics analysis were performed using genes screened by EPCI. For the x-cell algorithm, it can classify cells in the TME, including CAFs. However, during the calculation process, after filtering the common gene set and performing survival analysis, we found that the trend of high- and low-risk groups in the results of the x-cell algorithm was opposite. Therefore, we concluded that the gene set screened by x-cell algorithm was not suitable for subsequent research. Thus, we excluded this algorithm. Then, the tumor microenvironment was analyzed using the R package "estimate," which included stromal cell scoring. Fibroblast and stromal cell-scoring files were combined and exported. Differential analysis was carried out using the multiple R package "limma".

CAF scoring survival analysis

The clinical file, generated using TCGA and GEO databases, included patient ID, survival time, and survival status. We then combined and cycled the clinical, fibroblast-scoring, and TIDE-scoring files to obtain the optimal cut-off value, which was used to divide the clinical samples into the high- and low-risk groups. The high- and low-risk groups across all the data sets were then evaluated using the Kaplan-Meier (K-M) analysis in the "survival" R package to assess feasibility and analyze survival. Survival curves were plotted using the "survivor" and "surminer" in the R package (22).

WGCNA screen for CAF hub genes

From the integrated TCGA and GEO dataset files, the top 5000 genes with large fluctuations in expression were selected as reference for EPIC scoring. We used "WGCNA" in the R package to analyze all values, remove free values, and obtain the best power value (value = 8)

after conversion. Similar modules (number of genes = 30) were merged after clustering using a threshold of 0.2. Then, 1000 genes were randomly selected and used to draw a module gene heat map. Finally, a correlation heat map was constructed to illustrate the relationships between modules and CAF scoring. For the obtained modules and genes, a geneSigFilter value of 0.4 and a moduleSigFilter value of 0.8 were set, and the final hub genes of each module were output.

Functional enrichment analysis of the hub genes

Our GO analysis had three components: biological processes (BP), cellular components (CC), and molecular functions (MF). The biological functions of CC, MF, and BP target genes were obtained from the GO database(23). The Kyoto Encyclopedia of Genes and Genomes (KEGG) (https://www.kegg.jp/) incorporates chemical, genomic, and system functional information; it is a commonly utilized database for obtaining biological pathway information(24). Therefore, we utilized GO and KEGG analysis to analyze the signaling pathways and biological functions of the major enrichment of the intersecting hub genes using “clusterProfiler” in the R package.

Construction of prognosis-related hub genes model

After combining survival and gene expression data from TCGA, survival was analyzed using “survivor” and “survminer” in the R package. The one-way significance filter was set at $p \leq 0.05$, and core genes were cycled to find prognosis-related genes. Forest plots were drawn after extracting the expression of single-factor significant genes. Next, we used TCGA dataset as the training group and the GEO dataset as the test group to construct the prognostic model. The lasso regression model was constructed using “glmnet” in the R package to plot the cross-validation graph. We found the point with the lowest cross-validation error and outputted the model formula (gene expression level $*$ gene coefficient). Based on the median value of the sample risk score, the clinical samples were divided into high- and low-risk groups for subsequent analysis. Risk score = (0.0210157891801135 $*$ SERPINH1 expression level) + (0.110327492669992 $*$ COL5A1 expression level).

Survival analysis

To assess the predictive capacity of the model, K-M analysis of the high- and low-risk groups was conducted using “survival” in the R package. A variable was considered to be independently prognostic when the p-value for univariate and multivariate Cox regression

analysis was less than 0.05. K-M analysis was also used to determine the potential differences in progression-free survival (PFS) between the high- and low-risk groups.

Immunotherapy analysis and tumor mutation burden

Immunotherapy analysis was performed by inputting the TIDE file and using “plyr" in the R package(25). TIDE plot was then visualized, and the ROC curves were plotted. AUC values were calculated using “pROC” in the R package. Then, tumor mutation analysis and correlation with CAF scores were performed using “maftools” in the R package.

Drug sensitivity analysis

The Genomics of Drug Sensitivity in Cancer (GDSC) database (https://www.cancerrxgene.org/) is the largest public resource for tumor-cell drug sensitivity and anti-tumor therapeutic genomic data(26). Drug sensitivity was predicted for high- and low-risk groups by downloading the GDSC expression and drug-sensitivity files using the R packages “limma” and “ggpubr”. The filtering condition was set at $P < 0.05$. The lower the value of IC50, the higher the tumor sensitivity to the drug.

CCLE, HPA, and CGGA database validation

The Cancer Cell Line Encyclopedia (CCLE) is an open access database that contains multi-omics data on thousands of cancer-cell lines, and additional information that includes genetic mutations, RNA splicing, and protein modifications(27). From CCLE, we downloaded the GBM data; we also searched model genes for expression-verification data, which was then compared with fibroblast-expression data. The Human Protein Atlas (HPA) is an open access database based on proteomic, transcriptomic, and systems-biology data used to map tissues, cells, and organs. HPA includes not only tumor-related data, but also those on normal tissues. HPA additionally provides access to the survival curves of patients with cancer. In our present study, we used the HPA database to validate our model gene-expression maps in tumor and normal tissues. The Chinese Glioma Genome Atlas (CGGA) is also an open access database that uses genomic techniques combined with bioinformatics analysis to comprehensively map the glioma genome in the Chinese population. Here, we used the CGGA database to improve the integrity of the data on our model genes.

Cell culture and co-culture

The following cultured cell lines were used in this study: human normal astrocyte cell line SVGP12 (Hunan Fenghui Biotechnology Co., Ltd.), human GBM cell line U87 (GBM-like

cell, Hunan Fenghui Biotechnology Co., Ltd.), mouse GBM cell line G422-GFP-LUC (Hunan Fenghui Biotechnology Co., Ltd.), human GBM cell line T98G (Fuheng Co., Ltd.), human GBM cell line LN229 (Se Ou Biology Co., Ltd.), and human GBM cell line U343 (MeilunBio Co., Ltd.). The cells were expanded and cultured in Dulbecco's Modified Eagle Medium or Minimum Essential Medium supplemented with 100 u/mL penicillin/ streptomycin, and 10% fetal bovine serum (FBS). Cells were incubated at 37°C and a humidified atmosphere of 5% CO2. G422-GFP-LUC cells were selected using 1 μg/ml puromycin. All human cells were identified using short tandem repeat (STR) profiling, G422-GFP-LUC mouse species identification provided by the company (Hunan Fenghui Biotechnology Co., Ltd.). Cells were co-cultured using cell-culture plates with 0.4 μm transwell inserts (LABSELECT, LOT: 14112, PET, 24 mm, 0.4 μm). The upper chamber was seeded with SVGP12 cells, and the lower chamber was seeded with U87, T98G, LN229, or U343 cells. Cells in the upper and lower chamber were seeded at the density of 1.5 * 10^5. The upper chamber was placed into the corresponding wells after the cells had attached to the well. Cells were collected after 72 h of co-culture.

Cell function assay

Scratch assay was performed using six-well plates with 0.4 μm transwell chambers (LABSELECT, LOT: 14112, PET, 24 mm, 0.4 μm). SVGP12 cells were co-cultured with tumor cells for 72 h (1.5*10^5). After that, the chambers were rinsed three times with PBS pre-warmed at 37℃. Remove the chambers and place it on the inverted six - well plate lid. Draw lines using a 200μL pipette tip. Replace the chamber in the corresponding wells of the six - well plate after scratching. Rinse the chamber three times with PBS pre - warmed at 37℃, then add 2 mL of complete DMEM culture medium for incubation. Then, a wound healing assay was performed in the chambers for 0, 12, and 24 h. Migration experiments were performed using 12-well plates with 12 μm transwell chambers (JETBIOFIL, LOT: TCS100024, PC, 24 mm, 12 μm). SVGP12 cells were cultured in the upper chamber, while tumor cells were cultured in the lower chamber (1*10^5). The membrane between the transwell chambers was removed, and crystal violet staining and microscopy were performed after a 72 h co-culture.

Establishment of the GBM mouse model

Ten-week-old adult female BALB/c mice (18–22 g) were purchased from Guangdong Sijia Jinda Biotechnology Co. All procedures involving animals were approved by the Laboratory

Animal Ethics Committee of the Shantou University Medical College (SUMCSY2024-002, Material S1). Unfortunately, due to the strict ethical scrutiny of our research organization and the very small number of clinical cases, we do not have immediate access to human GBM tissue samples for our experiments. Additionally, in conducting the experimental design, we have considered normal brain samples as a control group. However, due to the strict ethical scrutiny of our research organization, we couldn't access to normal brain tissue for our experiments. Therefore, a mouse model was employed as a substitute.

Mice were housed in the animal center facility of the Shantou University Medical College. In this study, a total of 35 mice were used in the animal experiments. Among them, 21 mice were used for building GBM model and normal control, and the remaining normal mice were used as backups. Mice were anesthetized using tribromoethanol, and the fur on the heads was removed by shaving. The head of each mouse was immobilized using a rodent stereotaxic apparatus (RWD, 68025, China). The scalp was cut along the middle suture, and a burr hole was drilled into the skull (fontanel 2 mm to the right and 1 mm forward). G422-GFP-LUC cells (1*10^5) suspended in 5 ul saline were injected at 0.5 μl/min into the burr hole using a microsyringe extending 2 mm down from the opening. Preoperative (1 day) and postoperative (3, 7, 14 day) GBM mice were detected using a small animal in vivo imaging system (IVIS Kinetic, USA), using an intraperitoneal injection of fluorescein potassium salt (15 mg/ml PBS, ST196, Beyotime, China). Tumor tissues, peritumor tissues (According to the definition by Marc Aubry and colleagues, in this study, the peritumoral area of glioblastoma multiforme (GBM) is defined as the peripheral brain zone and the interface zone. During tissue sampling, the area within 2 - 3 mm of the tumour tissue, as assessed by microscopic examination, is considered peritumoral tissue(28).), and contralateral normal tissues were dissected using microscopy after the tumor had grown sufficiently.

Quantitative real-time PCR

The collected SVGP12 and tumor cells were lysed using Trizol to extract RNA, and cDNA was obtained by reverse transcription using a HiScript II First Strand cDNA Synthesis Kit (+gDNA Wiper) (Vazyme, China). RT-qPCR was carried out on an ABI 7500 Real Time PCR platform using ChamQ Universal SYBR qPCR Master Mix (Vazyme). The results were reliable when the Ct value was between 10 to 35. Changes in the expression of SERPINH1 and COL5A1 were detected. GAPDH was used as a reference gene. The $2^{-\Delta\Delta CT}$ method was used for data analysis. The primers used in this assay are listed in the Table S1.

Western blotting

The collected cells and animal tissues were lysed on ice for 30 min using RIPA buffer (Beyotime, P0013C) supplemented with 1 mM protease and phosphatase inhibitors (Beyotime, P1045), and centrifuged at 16900* g for 40 min. Supernatants were then collected. Electrophoresis was performed using 4–20% SDS-PAGE gels, and proteins were transferred onto a PVDF membrane (Millipore, Tullagreen, Carrigtwohill, Ireland). The membrane was blocked using 5% bovine serum albumin (BSA) (ST023, Beyotime, China) dissolved in TBST for 2 h and then incubated at 4°C overnight with the following primary antibodies specific for: SERPINH1 (sc-5293, Santa Cruz, 1:1000); COL5A1 (sc-133162, Santa Cruz, 1:1000); GAPDH (GB15002, Servicebio, 1:2000); AKT (#4685, CST, 1:1000); P-AKT (#4060, CST, 1:1000); mTor (ET1608-5, HUABIO, 1:1000); P-mTor (HA600094, HUABIO, 1:1000); FAP (AF5344, Affinity, 1:800); S100A4 (CY5799, Abways, 1:1000). The membrane was then incubated at 4°C for 3 h using the following secondary antibodies: HRP-labeled Goat Anti-Mouse IgG(H+L) (A0216, Beyotime, 1:1000) and HRP-labeled Goat Anti-Rabbit IgG(H+L) (A0208, Beyotime, 1:1000). Protein bands were visualized using ultra-high sensitivity ECL (BL520B, Biosharp, Anhui, China) and imaged using a Mini Chemi610 Mini Chemiluminescent Imaging and Analysis System (SINSAGE, Beijing, China). Photographs were taken using the instrument's own software (SageCaptur), and ImageJ was used to analyze the grayscale values. Images of full exposure membranes are shown in S1_raw_images.

Multicolor immunohistochemistry and HE staining

The mice were fully anesthetized using tribromoethanol and perfused using 4% paraformaldehyde. The brains were rapidly removed and placed into 4% paraformaldehyde for 48 h at 4°C. (G1101, Servicebio). Whole brains were embedded in paraffin and sectioned at the thickness of 3 μm (Leica, RM2235, German). Sections were affixed onto slides and stored at room temperature. Tissues were dewaxed (Xylene, 5 minutes, twice) and stained (75%–100% gradient alcohol, 5 minutes, once), using a using a four-color multiple fluorescent immunohistochemical staining kit (AFIHC024, AiFang Biological, Hunan, China), then incubated at 4°C overnight with the following primary antibodies specific for: SERPINH1 (sc-5293, Santa Cruz, 1:100); COL5A1 (WLH4136, Wanleibio, 1:100); GFAP (HA600094, HUABIO, 1:500); MBP (Wl03919, Wanleibi, 1:50); IBA1 (sc-32725, Santa Cruz, 1:100); FAP (AF5344, Affinity, 1:50); S100A4 (CY5799, Abways, 1:100). We also employed an anti-mouse/rabbit secondary antibody (AIFang, AFIHCC024). Imaging was

performed using a confocal microscope (ZEISS, LSM800, German). Whole-brain fluorescence scans were performed by Servicebio (Wuhan, China). Hematoxylin and eosin (HE) staining was carried out using a Hematoxylin and Eosin Staining Kit (C0105S, Beyotime), and scans were performed using an iScan Coreo slide scanner (Roche Diagnostics).

Ethical statement

All animal treatments and experiments in this study were approved by the Laboratory Animal Ethics Committee of Shantou University Medical College (The ethical review number: SUMCSY2024-002, Material S1).

Statistical analysis

All the bioinformatics analysis data were analyzed and visualized using R statistical programming language (version 4.2.3). The correlation matrix was constructed using Spearman's test. Differences were considered statistically significant at p-value less than 0.05. All experiments were repeated independently more than three times. GraphPad Prism 8 was used for statistical analysis, and Image J was used for image processing. For all experimental data, the Student's t-test was used for comparisons between two groups, while one-way ANOVA (analysis of variance) was employed for comparisons among multiple groups. All of the experiment was repeated three times, and the results are representative of three independent experiments. A p-value less than 0.05 was considered statistically significant. In the statistical figures, p-values are indicated with asterisks, where * represents $p < 0.05$, ** represents $p < 0.01$, *** represents $p < 0.001$, and **** represents $p < 0.0001$.

RESULTS

Identification of 2 CAF-related hub genes with prognostic significance

Drawing upon the established findings of prior research(29), we collected 606 samples (TCGA) and 50 samples (GEO) of GBM data from TCGA and GEO databases, respectively. The tumor samples contained clinical characteristics including age, sex, survival status, survival time, tumor grade IV, and mutation data. The 606 tumor samples from TCGA were used as the experimental group, and the 50 tumor samples from GEO were used as the control group for validation. These two datasets were scored using the following four algorithms: CAF-EPIC, CAF-MCPcounter, CAF-xCell and stromal cell scoring (Table S2 - S3). The two datasets were then classified into the high- and low-scoring groups based on

their respective score, and survival analysis was performed for each group. Except for the results obtained using CAF-xCell, the survival rates of the low-scoring group were better than those of the high-scoring group (Figure1A, B). This suggests that CAFs could effectively influence the prognosis of GBM. Next, we used WGCNA to find gene modules related to CAFs in the high- and low-scoring groups; we then extracted the core genes (Figure1C, D). We found the seven core genes (SERPINH1, LAMC1, LAMB1, COL5A2, ADAM12, COL5A1, COL6A2) by taking the intersection of the gene sets within the minimum p-value (Figure1E).

We combined seven hub genes with the survival data and constructed a forest map (Figure1F). A total of four prognostic-related high-risk genes (SERPINH1, LAMB1, COL5A1, COL6A2) were obtained. Based on the four hub genes, a prognosis-related model was constructed. Using the lasso regression model and cross-validation, we identified two hub genes (SERPINH1 and COL5A1) (Figure1G, H). Using these two hub genes, we performed a survival analysis using the two datasets, and found that the prognosis for the low-risk group was better than that for the high-risk group (Figure1I). This finding suggests that the model based on the two hub genes was successful and reflected the prognosis of patients with GBM. The CGGA-independent raw data analysis(30) system was used to validate the correlation between these two genes and the prognosis for patients with GBM in an external dataset. Our results indicate that SERPINH1 and COL5A1 showed increased expression in GBM (Figure S1, S2), which impacted the overall survival of patients with GBM (Figure1J, K). The result of the analysis in CGGA is detailed in Figure S3, S4.

Correlation analysis was performed to compare CAF scores with patient risk scores (Figure1L). All CAF scores were positively correlated with patient risk scores. The highest score (0.86) was obtained using an MCPcounter, indicating that CAF scores could be used as scoring criteria for GBM development. We also compared the CAF genes described in the published literature with the two hub genes identified in our present study. Our results indicate that the model genes showed consistent expression in the high-risk group, and showed positive correlation with the reported CAF-related genes in the literature (Figure1M, N). The two hub genes were consistent with the genes described in the published literature and showed the same predictive ability. We performed an immunotherapy analysis, tumor mutation and drug screen using these two hub genes. TIDE (Tumor Immune Dysfunction and Exclusion) is used to evaluate the potential clinical efficacy of immunotherapy in different risk groups and reflects the potential ability of tumor immune evasion. In our results, the

high-risk group had a higher TIDE score, which means the high-risk group had a higher immune evasion ability and worse immunotherapy outcomes (Figure S5). There was no significant difference between the high-and low-risk group when the total TMB was counted (Figure S5). The drug sensitivity showed that the top three drugs are daporinad, staurosporine, and sabutoclax. The details are described in Figure S5. In summary, we identified two CAF-related hub genes (SERPINH1, COL5A1) that may influence GBM prognosis.

SERPINH1 and *COL5A1* are highly expressed in the GBM and peritumor tissue

The Chinese Glioma Genome Atlas (CCLE) and Human Protein Atlas (HPA) databases were used to compare the expression of *SERPINH1* and *COL5A1* in normal and GBM tissues. Our results indicate that these two hub genes showed higher expression levels in fibroblasts compared with those in the GBM tissues from the CCLE database ($p < 0.05$, Figure 2A). In the HPA database, the protein expression of SERPINH1 and COL5A1 was higher in the tumor tissues than in normal tissues (Figure 2B, C). Next, we further evaluated the expression of these two genes in vivo. To simulate the complex microenvironment of the brain, we established an orthotopic G422-GFP-LUC GBM mouse model. Tumor implantation status was validated using bioluminescence imaging (Figure 2D). Results obtained using multi-color immunohistochemistry (mIHC) showed that protein expression of SERPINH1 and COL5A1 was increased in the tumor and peritumor tissues (Figure 2E, F). Elevated SERPINH1 and COL5A1 expression in mouse tumor tissues was consistent with the outcome shown in Figure 2b, c. To ensure the accuracy of the mIHC assay, the protein expression of SERPINH1 and COL5A1 in mouse peritumor tissues and normal tissue obtained from the opposite side of the same brain, was assessed using western blotting. Our results indicate that the expression of SERPINH1 and COL5A1 was higher in the peritumor tissue than in normal tissue (Figure 2I, t-test, $p < 0.05$, the statistical results are on the right side). This finding agrees with those obtained using IHC. Next, we used the two commonly used CAF markers, FAP and S100A4, to verify whether *SERPINH1* and *COL5A1* were specific CAF markers. IHC and western blotting showed that FAP and S100A4 were higher in the peritumor tissue than in normal tissue, which yielded the same results as those obtained for the expression of SERPINH1 and COL5A1 (Figure 2G, H, J, t-test, $p < 0.05$, the statistical results are on the right side). However, HE staining showed that there were normal brain tissue cells, no specific stained cells, and no specific pathological pattern in the peritumor tissue. (Figure 2K). This suggests that *SERPINH1* and *COL5A1* were indeed CAF-specific genes associated

with GBM, and that this particular expression profile may be responsible for some of the challenges involved in treating GBM. The statistical results are shown in Figure S7.

GBM peritumor tissues recruit GFAP-positive astrocytes expressing CAF-related proteins

To identify the cellular components of peritumor tissue in the GBM mouse model, multicolor IHC was used on whole-brain sections to label the expression of the three common types of glial cells: astrocytes, oligodendrocytes, and microglial cells. Interestingly, our study results indicate that, compared with normal brain tissue regions, the peritumoral tissues harbor 30% to 50% of microglia as previously documented in the literature (31) (Figure 3A-C, Figure S7, one-way ANOVA, $p < 0.05$). Concurrently, we also observed a substantial presence of astrocytes and a relatively small number of oligodendrocytes in the peritumoral tissues. (Figure 3A-C, Figure S7, one-way ANOVA, $p < 0.05$). Based on this finding, we postulated that the presence of a tumor may cause the migration and activation of astrocytes. To test this notion, we used a co-localization assay to evaluate the expression patterns of *SERPINH1* and *COL5A1*, and astrocytes (Figure 3D-G). Our results indicate that *SERPINH1* and *COL5A1* co-localized with GFAP-positive astrocytes that were abundantly present in the peritumor tissue. Notably, the results of co-localization assay used to assess the expression patterns of *FAP* and *S100A4*, and astrocytes, showed that *FAP* and *S100A4* were expressed not only in GFAP-positive astrocytes, but also in GFAP-negative astrocytes (Figure 3H-K, one-way ANOVA, $p < 0.05$). These findings suggest that the expression of *SERPINH1* and *COL5A1* was more specific to GFAP-positive astrocytes Therefore, we postulated that GBM recruited a large number of GFAP-positive astrocytes to the peritumor tissue during tumor development, and induced astrocytes to express CAF-related proteins. The statistical results are shown in Figure S7.

GBM cells recruit astrocytes and induce them to express CAF-related proteins

The mRNA and protein expression of SERPINH1 and COL5A1 in GBM cell lines and astrocytes (SVGP12), verified using RT-qPCR and western blotting (Figure 4A-B, one-way ANOVA, $p < 0.05$, the statistical results are on the right side), were inconsistent. The mRNA expression of SERPINH1 and COL5A1 was higher in SVGP12 than in GBM cell lines, but protein expression of SERPINH1 in LN229 was significantly higher than that in SVGP12 and other GBM cell lines (This may be attributed to post-transcriptional regulation). Thus, the mRNA and protein expression of SERPINH1 and COL5A1 were not specifically elevated in

GBM. To verify whether GBM induced astrocytes to express CAF-related proteins, a co-culture of human GBM cell lines and astrocytes was established using a transwell assay (Figure 4E). The expression of SERPINH1 and COL5A1 in the co-cultured cells was verified using RT-qPCR and western blotting. Compared with that in untreated SVGP12 cells, the mRNA and protein expression of SERPINH1 and COL5A1 was elevated in SVGP12 cells co-cultured with GBM cell lines (Figure 4C-D, one-way ANOVA, $p < 0.05$, the statistical results are on the right side). To verify whether GBM cells could recruit astrocytes, a wound healing and migration assays were used to assess SVGP12 cells in the co-cultured groups. Our wound healing assay shows that the scratch width in the co-cultured groups had narrowed significantly (Figure 4F, one-way ANOVA, $p < 0.05$, the statistical results are on the right side). The migration assay shows that in the co-cultured groups, an increased number of cells had migrated from the upper surface to the lower surface (Figure 4G, one-way ANOVA, $p < 0.05$, the statistical results are on the right side). These findings indicate that astrocytes in the co-cultured groups acquired an increased migration ability. In summary, these results suggest that GBM cells recruited astrocytes to the surrounding environment and induced the expression of CAF-related proteins in astrocytes. The statistical results are shown in Figure S7.

The AKT/m-TOR pathway mediates the induction of astrocytes by GBM cells

Pertinent to previous research, CAFs have their tumor-promoting effects in various cancer, and their activity is linked to an array of signaling pathways, notably PI3K/AKT/mTOR, WNT, and MAPK(32-34).To further investigate the aforementioned phenomenon, KEGG analysis was used to analyze the seven hub genes (*SERPINH1, LAMC1, LAMB1, COL5A2, ADAM12, COL5A1, COL6A2*). Our results show that these genes were enriched in the AKT pathway (Figure 5A). The AKT pathway regulates the growth, survival, proliferation, and migration of tumor cells. Protein expression of SERPINH1, COL5A1, p-AKT, and that of the downstream factor of p-AKT, p-mTOR, was detected in co-cultured SVGP12 cells using western blotting. Compared with that of the control group, the expression of p-AKT and p-mTOR was increased in the co-culture groups, whereas that of AKT and mTOR remained unchanged (Figure 5B, one-way ANOVA, $p < 0.05$, the statistical results are on the right side). These results indicate that GBM cells activated the AKT pathway in SVGP12 cells, which was followed by increased expression of SERPINH1 and COL5A1 in SVGP12 cells (Figure 4C, D, one-way ANOVA, $p < 0.05$, the statistical results are on the right side). Western blotting was performed in GBM mice. Our results indicate that the expression of p-

AKT and p-mTOR was increased in the peritumor tissue of these mice, whereas that of AKT and mTOR remained unchanged (Figure 5C, t-test, $p < 0.05$, the statistical results are on the right side). To verify the regulatory relationship between the two CAF-specific genes (*SERPINH1* and *COL5A1*) and the AKT pathway, the AKT agonist sc79 was used to treat SVGP12 cells, and the AKT inhibitor perifosine was used to treat the co-cultured SVGP12 cells. Our results indicate that when p-AKT was activated in SVGP12 cells, the expression of SERPINH1 and COL5A1 was elevated (Figure 5D, t-test, $p < 0.05$,the statistical results are below the figure), and the migratory ability of SVGP12 cells was enhanced (Figure 5E). Conversely, when p-AKT was inhibited in co-cultured SVGP12 cells, the expression of SERPINH1 and COL5A1 was reduced (Figure5F-G, one-way ANOVA, $p < 0.05$, the statistical results are on the right side). In summary, our result show that GBM recruited astrocytes to the peritumor tissue and induced them to express the CAF-related proteins SERPINH1 and COL5A1 via the AKT pathway, which suggest that astrocytes may be a potential source of CAF precursor cells in the tumor microenvironment of GBM. The statistical results are shown in Figure S7.

DISCUSSION

Glioblastoma multiforme (GBM) is the most malignant type of glioma. Although the development of science and technology has spurred some advances in the treatment of glioma, there is currently no cure, and the prognosis of patients with glioma remains poor(35). GBM is highly invasive, even when the tumor is completely resected with adjuvant chemotherapy; this invasiveness presents one of the main challenges in the treatment of patients with glioma. GBM recurs mainly in, or within a few centimeters of, the resection cavity(36, 37). Much of the invasiveness and intractability of GBM also stems from its microenvironment(38). Cancer-associated fibroblasts (CAFs), which are indispensable components of this microenvironment, play a variety of roles(15). However, GBM differs from other types of tumors. Several studies have shown that there are no fibroblasts in the brain, except for a small number of fibroblasts in the vasculature of the brain(39). Evidence also suggests that CAFs do not originate from tumor-invaded peripheral cells, but instead originate from other cells in the surrounding environment such as bone marrow-derived precursor cells or mesenchymal stem cells(40-43). Therefore, the presence of CAFs in GBM is plausible. Several studies have identified cells that express CAF-associated markers in GBM; however, there are no gene-expression profiles confirming that these cells are indeed CAFs and no evidence showing their role in the biology of GBM(44-46). Although in situ

injection of GBM is already a well-established mouse model of GBM, this study represented a novel attempt to observe the distribution of CAFs in the whole brain of GBM.

In our present study, TCGA and GEO data were combined, and a prognosis-related model was constructed using four CAF-related genes. Using this prognostic model, we determined that the survival of patients with GBM was associated with the CAF score. Using WGCNA, *SERPINH1*, and *COL5A1* were identified as CAF-related hub genes that can be used to predict the survival prognosis of patients with GBM.

SERPINH1, a member of the serine protease inhibitor superfamily, encodes heat shock protein 47, which functions as a collagen-specific molecular chaperone. SERPINH1 is abnormally expressed in various cancers and is associated with their malignant progression, potentially serving as a prognostic marker for cancer(47). Existing literature has indicated that SERPINH1 is associated with the prognosis of various cancers, including glioblastoma (GBM), gastric cancer, and lung cancer(48-50). SERPINH1, acting as an oncogene, is involved in the occurrence and progression of glioma. Inhibiting SERPINH1 can effectively suppress the proliferation, migration, and invasion of glioma cells and induce apoptosis. Knockout of SERPINH1 in vivo can effectively inhibit tumor growth(51). As a novel prognostic biomarker for glioma, SERPINH1 promotes tumor progression via pathways such as JAK-STAT and interacts with the immune microenvironment. High SERPINH1 expression is linked to enhanced immune evasion and poor immunotherapy outcomes, offering a new target for personalized treatment(52). And SERPINH1 is positively correlated with immune cells and immune checkpoint molecules. This suggests its oncogenic role may be associated with impaired tumor immune function and indicates potential value in immunotherapy(52). Thus, further research is needed to investigate the role of SERPINH1 in glioma progression.

COL5A1 (Type Vα1 collagen), a collagen protein, participates in the formation of the extracellular matrix(53). The product of COL5A1, a fibril-forming collagen, is a component of the extracellular matrix and is closely related to type XI collagen. Type V and XI collagen chains may form a single collagen type with tissue-specific chain combinations. Additionally, COL5A1 has been reported to be associated with hypoxia(54). Collagen deposition is typically considered a pathological feature of TME(55). Additionally, chemoresistance is associated with increased tissue stiffness mediated by specific collagen crosslinking(56). It is reported that COL5A1 is highly expressed in multiple cancers and is negatively correlated

with prognosis in various cancers(57, 58). COL5A1 is co-expressed with genes encoding the major histocompatibility complex, immune activators, immune suppressors, chemokines, chemokine receptors, mismatch repair genes, and immune checkpoints(57). However, the role of COL5A1 in human cancers remains unclear. More efforts are needed to elucidate its function in human tumors.

In order to investigate the effects of SERPINH1 and COL5A1 on GBM, we established an orthotopic GBM mouse model to simulate the complex brain microenvironment, and to validate the expression of these two genes. SERPINH1 and COL5A1 showed increased expression in the peritumor tissue and were highly co-localized in the surrounding astrocytes. This finding can be explained using our in-vitro studies, showing that astrocytes were recruited to the peritumor tissue by GBM. Additionally, these GBM-recruited astrocytes expressed the CAF-associated proteins SERPINH1 and COL5A1 via the AKT pathway, and may have exerted CAF-like effects. Several studies have examined SERPINH1 and COL5A1 in the context of GBM. However, to the best of our knowledge, our present study is the first to identify *SERPINH1* and *COL5A1* using CAF scores and predict their biological effects. Our GO and KEGG enrichment analysis showed that *SERPINH1* and *COL5A1* were mainly enriched in glial cell formation and construction, and ECM. In lieu of the absence of visible fibroblasts in the brain(59, 60), our findings suggest that astrocytes could serve as a potential origin for CAFs. We postulated that changes in the expression of *SERPINH1* and *COL5A1* may trigger astrocytes to exert CAF-like effects, and may also regulate the invasiveness and metastasis of tumors. Under physiological conditions, astrocytes perform a variety of functions, including providing trophic and mechanical support to neurons, promoting synaptogenesis and maintaining normal synaptic function, pruning synapses through phagocytosis, contributing to the formation of the blood-brain barrier, and participating in other homeostatic maintenance functions(61). In our research, we observed that a large number of astrocytes were recruited in the peritumoral tissues, which expressed CAF-related factors, SERPINH1 and COL5A1. We speculate that the recruited astrocytes may exert CAF-associated functions, contributing to the therapeutic resistance and recurrence of glioma. It has been discovered that astrocytes can be activated into two distinct polarization states: the neurotoxic or pro-inflammatory phenotype (A1) and the neuroprotective or anti-inflammatory phenotype (A2)(62). A1 astrocytes produce neurotoxic and pro-inflammatory cytokines, which contribute to the progression of neuronal injury. In contrast, A2 astrocytes can release anti-inflammatory cytokines and neurotrophic factors(63). Due to limitations in experimental

conditions, we are currently unable to further validate the phenotype of these astrocytes. In recent reports, A1-type astrocytes have been shown to have close connections with glioma cells, and A1 astrocytes regulate tumor and microenvironmental cells through cell-to-cell contact or the secretion of bioactive substances(64). Therefore, we speculate that the recruitment of astrocytes in the peritumoral tissues may be of the A1 subtype, which may be involved in the progression of glioma.

In this study, we also used MCPcounter as scoring methods (Figure S6). Although numerous hub genes were available, EPIC and MCPcounter indicated that the most common genes were *SERPINH1* and *COL5A1*.Therefore, *SERPINH1* and *COL5A1* were considered. Model construction and subsequent bioinformatics analysis were performed using genes screened by EPCI. For the x-cell algorithm, we initially used three well - recognized CAF scoring algorithms, which can classify cells in the TME, including CAFs. However, during the calculation process, after filtering the common gene set and performing survival analysis, we found that the trend of high- and low-risk groups in the results of the x-cell algorithm was opposite. Therefore, we concluded that the gene set screened by this algorithm was not suitable for subsequent research. Thus, we excluded this algorithm.

In our study, although astrocytes may represent precursor cells of CAFs in GBM, their specific role in the GBM immune microenvironment remains unclear. Our bioinformatics analysis revealed that the high-risk group exhibited higher TIDE scores, and literature reports indicate that CAFs play an immunosuppressive role in tumor progression(65). Thus, these CAFs-like astrocytes may exert immunosuppressive effects, a hypothesis that warrants further experimental validation. Using TMB analysis, we found that CAFs exerted no significant effects on GBM mutations, which was consistent with the prognosis results obtained using CGGA. This finding indicates that the accuracy of our prognostic results was high. For the overall prognostic analysis, our data were sourced from Europe, America, and Japan. Additionally, all data were grade IV GBM; however, survival prognosis using both genes (*SERPINH1* and *COL5A1*) from CGGA was more inclined toward grade III GBM, which may be related to patient ethnicity or geographic setting.

During our research, Western blot analysis of SERPINH1 and COL5A1 revealed multiple bands, potentially due to protein degradation, subtypes/splice variants, or antibody cross-reactivity. We employed the widely accepted AKT inhibitor Perifosine to investigate changes in SERPINH1 and COL5A1. Results showed that inhibiting the AKT pathway reduced

SERPINH1 and COL5A1 protein expression in astrocytes and affected their migration capacity. Specific bands for SERPINH1 and COL5A1 are indicated by the red arrows in Figure 4C.

In conclusion, we used CAF scores to analyze the GBM data from different sources. We identified two CAF-related genes that affected the prognosis of GBM. This finding may provide valuable information for the development of future targeted therapeutics. We believe that this study will provide new insights into the molecular therapeutic implications of CAF in GBM. Through our study, the distribution of CAF-like astrocytes can be localized by SERPINH1/COL5A1 to identify the extent of the tumor more precisely during the diagnosis and treatment of GBM. Moreover, it may be possible to increase the efficacy of AKT-inhibiting drugs against GBM by modulating SERPINH1/COL5A1.Although the findings obtained in our present study advance the understanding of GBM, our study had several limitations. Determining whether *SERPINH1* and *COL5A1* directly affected the survival prognosis of GBM was necessary to perform the experimental analysis, and the more precise and numerous samples originating from human tissues were required, rather than a single cell line. Additionally, although bioinformatics was used as a predictive tool, the sources and formation of CAFs in GBM need to be proven by extensive in-vivo and in-vitro studies. Moreover, the role of CAFs in GBM is still not fully explained. Some studies have shown that CAFs have different effects on tumors, promoting(66, 67) or inhibiting(68, 69) tumor growth, but this activity seems to be occurring through a different pathway. Although our work elucidated the effect of GBM on astrocytes, we did not investigate the effect of astrocytes on GBM after the changes had occurred, which represents a future line of research.

CONCLUSION

In our study, two CAF-related genes, SERPINH1 and COL5A1, were identified in the GBM datasets and may affect the prognosis of GBM patients. Our findings indicate that these two genes were highly expressed in the peritumor tissue. We also found that GBM could recruit astrocytes to the peritumor tissue via activation of the AKT/mTOR pathway. GBM also induced these recruited astrocytes to express CAF-related proteins (SERPINH1 and COL5A1). Our results suggest that astrocytes may be a potential source of CAF precursor cells in the tumor microenvironment of GBM. Therefore, the distribution of CAF-like astrocytes can be localized by SERPINH1/COL5A1 to identify the extent of the tumor more precisely during the diagnosis and treatment of GBM. Moreover, it may be possible to

increase the efficacy of AKT-inhibiting drugs against GBM by modulating SERPINH1/COL5A1.

ACKNOWLEDGMENTS

The authors gratefully acknowledge databases, such as TCGA, GEO, CGGA, HPA, CCLE for offering convenient access to datasets. We thank Professor Stanley Lin for modifying the article. We thank LetPub (www.letpub.com.cn) for linguistic assistance (Material S2).

Conflicts of interest: Authors declare no conflicts of interest.

Funding: This work was supported by The Tenth Affiliated Hospital, Southern Medical University（Dongguan People's Hospital), (Grant No. G202410); Teaching Reform Research Program of Clinical Teaching Base of Guangdong Province (〔2022〕21-2021JD066), the Medical Scientific Research Foundation of Guangdong Province of China (Grant No. A2022176), Li Ka Shing Foundation Cross-Disciplinary Research Grant (2020LKSFG03B).

Data availability: We have uploaded the code and data from the manuscript to a database. The link and schematic representation are in Material S3.

Submitted: 20 December 2024

Accepted: 27 May 2025

Published online: 12 June 2025

REFERENCES

1. Tan AC, Ashley DM, López GY, Malinzak M, Friedman HS, Khasraw M. Management of glioblastoma: State of the art and future directions. CA: a cancer journal for clinicians. 2020;70(4):299-312.
2. Vargas López AJ. Glioblastoma in adults: a Society for Neuro-Oncology (SNO) and European Society of Neuro-Oncology (EANO) consensus review on current management and future directions. Neuro-oncology. 2021;23(3):502-3.
3. Phillips HS, Kharbanda S, Chen R, Forrest WF, Soriano RH, Wu TD, et al. Molecular subclasses of high-grade glioma predict prognosis, delineate a pattern of disease progression, and resemble stages in neurogenesis. Cancer cell. 2006;9(3):157-73.
4. Wesolowski JR, Rajdev P, Mukherji SK. Temozolomide (Temodar). AJNR American journal of neuroradiology. 2010;31(8):1383-4.

5. Chen J, Li Y, Yu TS, McKay RM, Burns DK, Kernie SG, et al. A restricted cell population propagates glioblastoma growth after chemotherapy. Nature. 2012;488(7412):522-6.
6. De Vleeschouwer S, Bergers G. Glioblastoma: To Target the Tumor Cell or the Microenvironment? In: De Vleeschouwer S, editor. Glioblastoma. Brisbane (AU): Codon Publications
Copyright: The Authors.; 2017.
7. Jinushi M, Chiba S, Yoshiyama H, Masutomi K, Kinoshita I, Dosaka-Akita H, et al. Tumor-associated macrophages regulate tumorigenicity and anticancer drug responses of cancer stem/initiating cells. Proceedings of the National Academy of Sciences of the United States of America. 2011;108(30):12425-30.
8. Lau EY, Ho NP, Lee TK. Cancer Stem Cells and Their Microenvironment: Biology and Therapeutic Implications. Stem cells international. 2017;2017:3714190.
9. Bilotta MT, Antignani A, Fitzgerald DJ. Managing the TME to improve the efficacy of cancer therapy. Frontiers in immunology. 2022;13:954992.
10. Bhat KPL, Balasubramaniyan V, Vaillant B, Ezhilarasan R, Hummelink K, Hollingsworth F, et al. Mesenchymal differentiation mediated by NF-κB promotes radiation resistance in glioblastoma. Cancer cell. 2013;24(3):331-46.
11. Hara T, Chanoch-Myers R, Mathewson ND, Myskiw C, Atta L, Bussema L, et al. Interactions between cancer cells and immune cells drive transitions to mesenchymal-like states in glioblastoma. Cancer cell. 2021;39(6):779-92.e11.
12. Pietras A, Katz AM, Ekström EJ, Wee B, Halliday JJ, Pitter KL, et al. Osteopontin-CD44 signaling in the glioma perivascular niche enhances cancer stem cell phenotypes and promotes aggressive tumor growth. Cell stem cell. 2014;14(3):357-69.
13. Madar S, Goldstein I, Rotter V. 'Cancer associated fibroblasts'--more than meets the eye. Trends in molecular medicine. 2013;19(8):447-53.
14. Kalluri R. The biology and function of fibroblasts in cancer. Nature reviews Cancer. 2016;16(9):582-98.
15. Buchsbaum RJ, Oh SY. Breast Cancer-Associated Fibroblasts: Where We Are and Where We Need to Go. Cancers. 2016;8(2).
16. Sahai E, Astsaturov I, Cukierman E, DeNardo DG, Egeblad M, Evans RM, et al. A framework for advancing our understanding of cancer-associated fibroblasts. Nature reviews Cancer. 2020;20(3):174-86.
17. Park D, Sahai E, Rullan A. SnapShot: Cancer-Associated Fibroblasts. Cell. 2020;181(2):486-.e1.
18. Feng B, Wu J, Shen B, Jiang F, Feng J. Cancer-associated fibroblasts and resistance to anticancer therapies: status, mechanisms, and countermeasures. Cancer cell international. 2022;22(1):166.
19. Galbo PM, Jr., Madsen AT, Liu Y, Peng M, Wei Y, Ciesielski MJ, et al. Functional Contribution and Clinical Implication of Cancer-Associated Fibroblasts in Glioblastoma. Clin Cancer Res. 2024;30(4):865-76.
20. Jiang P, Gu S, Pan D, Fu J, Sahu A, Hu X, et al. Signatures of T cell dysfunction and exclusion predict cancer immunotherapy response. Nature medicine. 2018;24(10):1550-8.
21. Wang X, Xie C, Lin L. Development and validation of a cuproptosis-related lncRNA model correlated to the cancer-associated fibroblasts enable the prediction prognosis of patients with osteosarcoma. Journal of bone oncology. 2023;38:100463.
22. Mayakonda A, Lin DC, Assenov Y, Plass C, Koeffler HP. Maftools: efficient and comprehensive analysis of somatic variants in cancer. Genome Res. 2018;28(11):1747-56.

23. Ashburner M, Ball CA, Blake JA, Botstein D, Butler H, Cherry JM, et al. Gene ontology: tool for the unification of biology. The Gene Ontology Consortium. Nature genetics. 2000;25(1):25-9.
24. Kanehisa M, Goto S. KEGG: kyoto encyclopedia of genes and genomes. Nucleic acids research. 2000;28(1):27-30.
25. Noblejas-López MDM, Nieto-Jiménez C, Morcillo García S, Pérez-Peña J, Nuncia-Cantarero M, Andrés-Pretel F, et al. Expression of MHC class I, HLA-A and HLA-B identifies immune-activated breast tumors with favorable outcome. Oncoimmunology. 2019;8(10):e1629780.
26. Yang W, Soares J, Greninger P, Edelman EJ, Lightfoot H, Forbes S, et al. Genomics of Drug Sensitivity in Cancer (GDSC): a resource for therapeutic biomarker discovery in cancer cells. Nucleic acids research. 2013;41(Database issue):D955-61.
27. Nusinow DP, Szpyt J, Ghandi M, Rose CM, McDonald ER, 3rd, Kalocsay M, et al. Quantitative Proteomics of the Cancer Cell Line Encyclopedia. Cell. 2020;180(2):387-402.e16.
28. Aubry M, de Tayrac M, Etcheverry A, Clavreul A, Saikali S, Menei P, et al. From the core to beyond the margin: a genomic picture of glioblastoma intratumor heterogeneity. Oncotarget. 2015;6(14):12094-109.
29. Shi Y, Kong Z, Liu P, Hou G, Wu J, Ma W, et al. Oncogenesis, Microenvironment Modulation and Clinical Potentiality of FAP in Glioblastoma: Lessons Learned from Other Solid Tumors. Cells. 2021;10(5).
30. Zhao Z, Zhang KN, Wang Q, Li G, Zeng F, Zhang Y, et al. Chinese Glioma Genome Atlas (CGGA): A Comprehensive Resource with Functional Genomic Data from Chinese Glioma Patients. Genomics, proteomics & bioinformatics. 2021;19(1):1-12.
31. Andersen RS, Anand A, Harwood DSL, Kristensen BW. Tumor-Associated Microglia and Macrophages in the Glioblastoma Microenvironment and Their Implications for Therapy. Cancers. 2021;13(17).
32. Pang T, Yin X, Luo T, Lu Z, Nie M, Yin K, et al. Cancer-associated fibroblasts promote malignancy of gastric cancer cells via Nodal signalling. Cell Biochem Funct. 2020;38(1):4-11.
33. Ishii G, Hashimoto H, Asada K, Ito T, Hoshino A, Fujii S, et al. Fibroblasts associated with cancer cells keep enhanced migration activity after separation from cancer cells: a novel character of tumor educated fibroblasts. Int J Oncol. 2010;37(2):317-25.
34. Zhou L, Yang K, Randall Wickett R, Zhang Y. Dermal fibroblasts induce cell cycle arrest and block epithelial-mesenchymal transition to inhibit the early stage melanoma development. Cancer Med. 2016;5(7):1566-79.
35. Davis ME. Epidemiology and Overview of Gliomas. Seminars in oncology nursing. 2018;34(5):420-9.
36. Niyazi M, Brada M, Chalmers AJ, Combs SE, Erridge SC, Fiorentino A, et al. ESTRO-ACROP guideline "target delineation of glioblastomas". Radiotherapy and oncology : journal of the European Society for Therapeutic Radiology and Oncology. 2016;118(1):35-42.
37. Lemée JM, Clavreul A, Menei P. Intratumoral heterogeneity in glioblastoma: don't forget the peritumoral brain zone. Neuro-oncology. 2015;17(10):1322-32.
38. Quail DF, Joyce JA. The Microenvironmental Landscape of Brain Tumors. Cancer cell. 2017;31(3):326-41.
39. LeBleu VS, Neilson EG. Origin and functional heterogeneity of fibroblasts. FASEB journal : official publication of the Federation of American Societies for Experimental Biology. 2020;34(3):3519-36.

40. Direkze NC, Hodivala-Dilke K, Jeffery R, Hunt T, Poulsom R, Oukrif D, et al. Bone marrow contribution to tumor-associated myofibroblasts and fibroblasts. Cancer research. 2004;64(23):8492-5.
41. Jung Y, Kim JK, Shiozawa Y, Wang J, Mishra A, Joseph J, et al. Recruitment of mesenchymal stem cells into prostate tumours promotes metastasis. Nature communications. 2013;4:1795.
42. Mishra PJ, Mishra PJ, Humeniuk R, Medina DJ, Alexe G, Mesirov JP, et al. Carcinoma-associated fibroblast-like differentiation of human mesenchymal stem cells. Cancer research. 2008;68(11):4331-9.
43. Quante M, Tu SP, Tomita H, Gonda T, Wang SS, Takashi S, et al. Bone marrow-derived myofibroblasts contribute to the mesenchymal stem cell niche and promote tumor growth. Cancer cell. 2011;19(2):257-72.
44. Clavreul A, Etcheverry A, Chassevent A, Quillien V, Avril T, Jourdan ML, et al. Isolation of a new cell population in the glioblastoma microenvironment. Journal of neuro-oncology. 2012;106(3):493-504.
45. Clavreul A, Guette C, Faguer R, Tétaud C, Boissard A, Lemaire L, et al. Glioblastoma-associated stromal cells (GASCs) from histologically normal surgical margins have a myofibroblast phenotype and angiogenic properties. The Journal of pathology. 2014;233(1):74-88.
46. Trylcova J, Busek P, Smetana K, Jr., Balaziova E, Dvorankova B, Mifkova A, et al. Effect of cancer-associated fibroblasts on the migration of glioma cells in vitro. Tumour biology : the journal of the International Society for Oncodevelopmental Biology and Medicine. 2015;36(8):5873-9.
47. Wang Y, Gu W, Wen W, Zhang X. SERPINH1 is a Potential Prognostic Biomarker and Correlated With Immune Infiltration: A Pan-Cancer Analysis. Frontiers in genetics. 2021;12:756094.
48. Zhang H, Yan X, Gu H, Xue Q, Liu X. High SERPINH1 expression predicts poor prognosis in lung adenocarcinoma. Journal of thoracic disease. 2022;14(12):4785-802.
49. Li T, Gao X, Han L, Yu J, Li H. Identification of hub genes with prognostic values in gastric cancer by bioinformatics analysis. World journal of surgical oncology. 2018;16(1):114.
50. Zhang S, Zhang W, Wu B, Xia L, Li L, Jin K, et al. Hub gene target of glioblastoma: LOX, SERPINH1 and TGFBI. Medicine. 2022;101(45):e31418.
51. Wang Q, Wang Z. Serpin family H member 1 and its related collagen gene network are the potential prognostic biomarkers and anticancer targets for glioma. Journal of biochemical and molecular toxicology. 2024;38(1):e23541.
52. Hou S, Chen Y, Jin C, Lin N. Integrative analysis of bulk RNA-seq and scRNA-seq data indicates the prognostic and immunologic values of SERPINH1 in glioma. Environmental toxicology. 2024;39(6):3654-65.
53. An F, Zhang Z, Xia M, Xing L. Subpath analysis of each subtype of head and neck cancer based on the regulatory relationship between miRNAs and biological pathways. Oncology reports. 2015;34(4):1745-54.
54. Jiang M, Ren L, Chen Y, Wang H, Wu H, Cheng S, et al. Identification of a Hypoxia-Related Signature for Predicting Prognosis and the Immune Microenvironment in Bladder Cancer. Frontiers in molecular biosciences. 2021;8:613359.
55. Martins Cavaco AC, Dâmaso S, Casimiro S, Costa L. Collagen biology making inroads into prognosis and treatment of cancer progression and metastasis. Cancer metastasis reviews. 2020;39(3):603-23.

56. Sinha S, Fleck M, Ayushman M, Tong X, Mikos G, Jones S, et al. Matrix Stiffness Regulates GBM Migration and Chemoradiotherapy Responses via Chromatin Condensation in 3D Viscoelastic Matrices. ACS applied materials & interfaces. 2025;17(7):10342-59.
57. Zhu H, Hu X, Feng S, Jian Z, Xu X, Gu L, et al. The Hypoxia-Related Gene COL5A1 Is a Prognostic and Immunological Biomarker for Multiple Human Tumors. Oxidative medicine and cellular longevity. 2022;2022:6419695.
58. Ucaryilmaz Metin C, Ozcan G. Comprehensive bioinformatic analysis reveals a cancer-associated fibroblast gene signature as a poor prognostic factor and potential therapeutic target in gastric cancer. BMC cancer. 2022;22(1):692.
59. Tian S, Peng P, Li J, Deng H, Zhan N, Zeng Z, et al. SERPINH1 regulates EMT and gastric cancer metastasis via the Wnt/β-catenin signaling pathway. Aging. 2020;12(4):3574-93.
60. Zhao B, Song X, Guan H. CircACAP2 promotes breast cancer proliferation and metastasis by targeting miR-29a/b-3p-COL5A1 axis. Life sciences. 2020;244:117179.
61. Barsanti S, Viana JF, Veiga A, Machado JL, Abreu DS, Dias JD, et al. Assessing Different Histological Preparations for Reconstruction of Astrocyte Tridimensional Structure. Cells. 2024;13(11).
62. Abulaban AA, Al-Kuraishy HM, Al-Gareeb AI, Albuhadily AK, Shokr MM, Alexiou A, et al. The janus face of astrocytes in multiple sclerosis: Balancing protection and pathology. Brain research bulletin. 2025;226:111356.
63. Wang J, Cheng C, Liu Z, Lin Y, Yang L, Zhang Z, et al. Inhibition of A1 Astrocytes and Activation of A2 Astrocytes for the Treatment of Spinal Cord Injury. Neurochemical research. 2023;48(3):767-80.
64. Wu J, Li R, Wang J, Zhu H, Ma Y, You C, et al. Reactive Astrocytes in Glioma: Emerging Opportunities and Challenges. International journal of molecular sciences. 2025;26(7).
65. Di Spirito A, Balkhi S, Vivona V, Mortara L. Key immune cells and their crosstalk in the tumor microenvironment of bladder cancer: insights for innovative therapies. Exploration of targeted anti-tumor therapy. 2025;6:1002304.
66. Hanahan D, Weinberg RA. Hallmarks of cancer: the next generation. Cell. 2011;144(5):646-74.
67. Liao D, Luo Y, Markowitz D, Xiang R, Reisfeld RA. Cancer associated fibroblasts promote tumor growth and metastasis by modulating the tumor immune microenvironment in a 4T1 murine breast cancer model. PLoS One. 2009;4(11):e7965.
68. Stoker MG, Shearer M, O'Neill C. Growth inhibition of polyoma-transformed cells by contact with static normal fibroblasts. J Cell Sci. 1966;1(3):297-310.
69. Dotto GP, Weinberg RA, Ariza A. Malignant transformation of mouse primary keratinocytes by Harvey sarcoma virus and its modulation by surrounding normal cells. Proc Natl Acad Sci U S A. 1988;85(17):6389-93.

FIGURES WITH LEGENDS

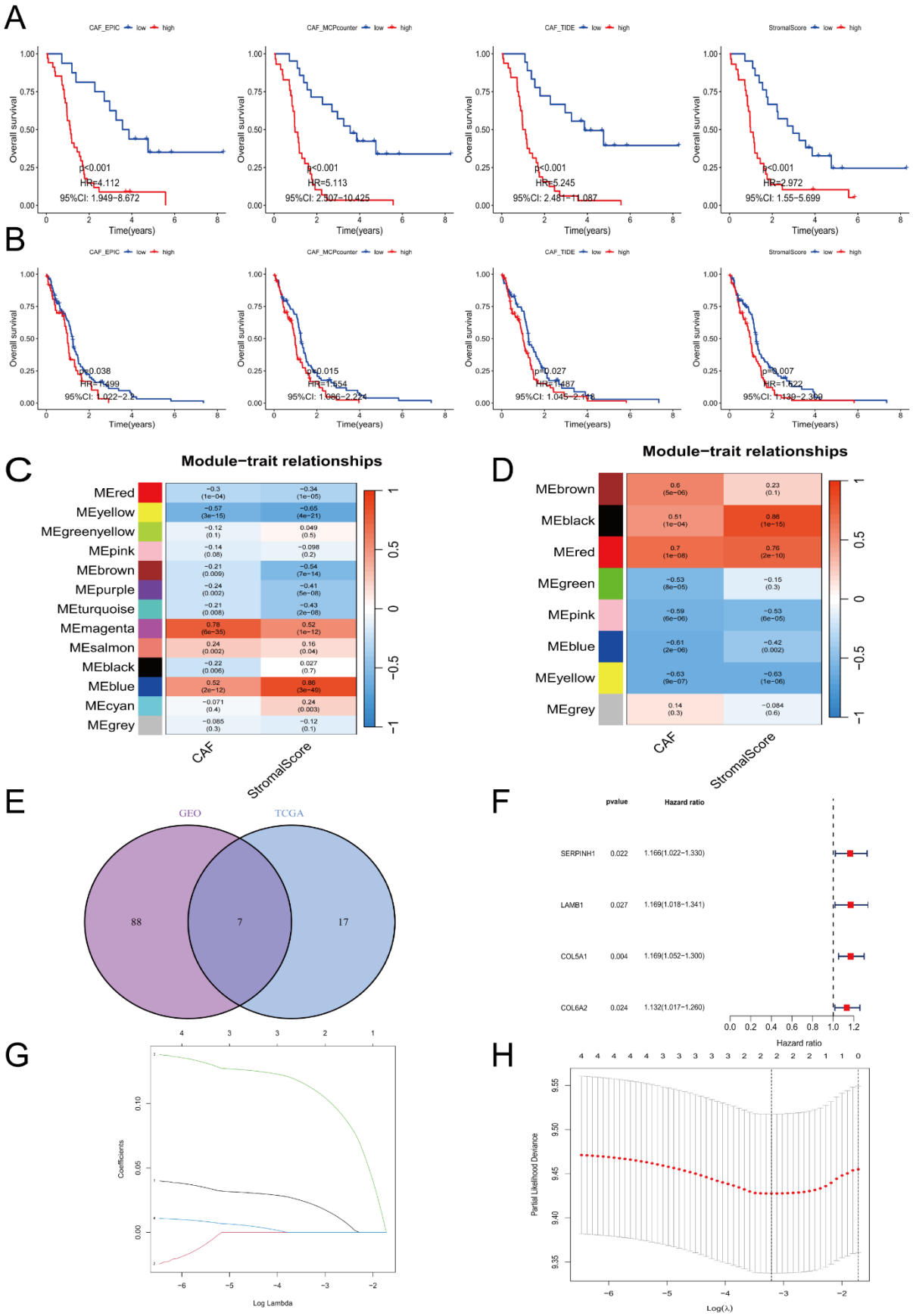

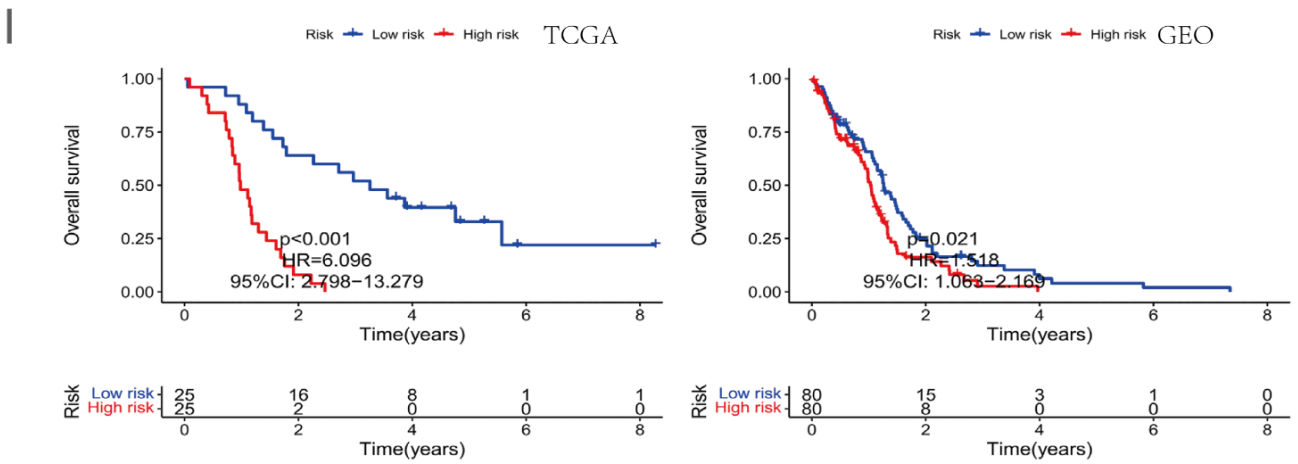
I
Risk Low risk High risk TCGA
Overall survival
p<0.001
HR=6.096
95%CI: 2.798−13.279
Time(years)
Risk Low risk High risk GEO
Overall survival
p=0.021
HR=1.518
95%CI: 1.063−2.169
Time(years)
Risk Low risk 25 16 8 1 1
High risk 25 2 0 0 0
Time(years)
Risk Low risk 80 15 3 1 0
High risk 80 8 0 0 0
Time(years)

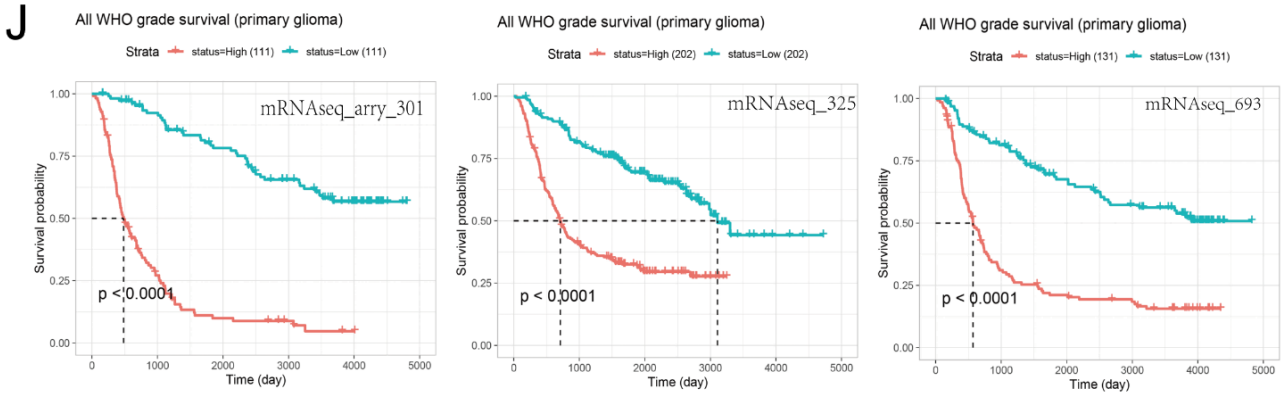
J
All WHO grade survival (primary glioma)
Strata status=High (111) status=Low (111)
mRNAseq_arry_301
Survival probability
p < 0.0001
Time (day)
All WHO grade survival (primary glioma)
Strata status=High (202) status=Low (202)
mRNAseq_325
Survival probability
p < 0.0001
Time (day)
All WHO grade survival (primary glioma)
Strata status=High (131) status=Low (131)
mRNAseq_693
Survival probability
p < 0.0001
Time (day)

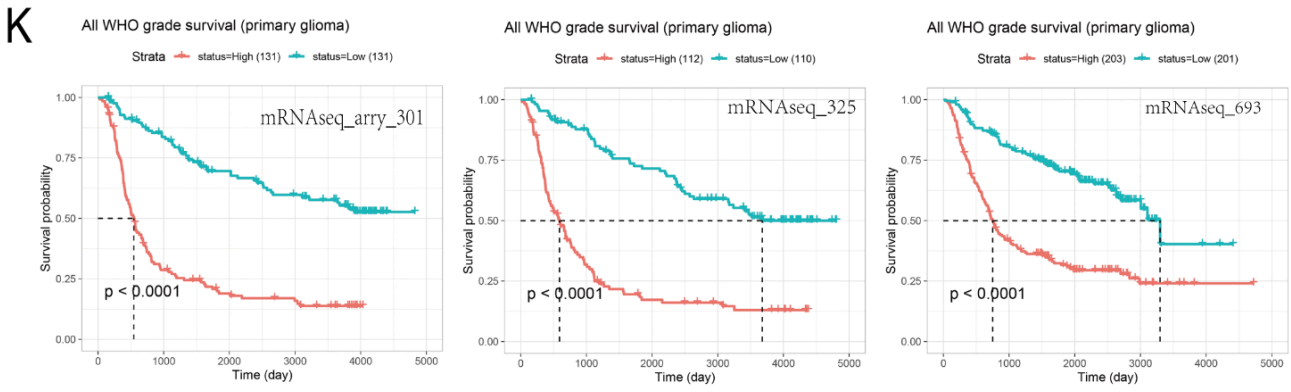
K
All WHO grade survival (primary glioma)
Strata status=High (131) status=Low (131)
mRNAseq_arry_301
Survival probability
p < 0.0001
Time (day)
All WHO grade survival (primary glioma)
Strata status=High (112) status=Low (110)
mRNAseq_325
Survival probability
p < 0.0001
Time (day)
All WHO grade survival (primary glioma)
Strata status=High (203) status=Low (201)
mRNAseq_693
Survival probability
p < 0.0001
Time (day)

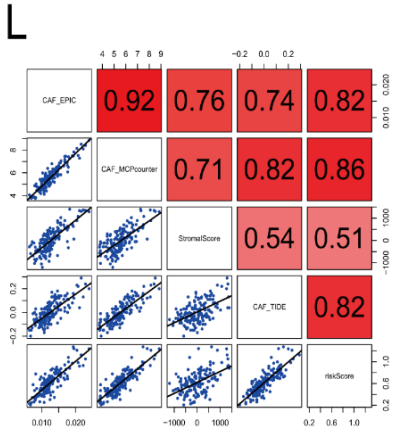
L
CAF_EPIC
CAF_MCPcounter
StromalScore
CAF_TIDE
riskScore
0.92
0.76
0.74
0.82
0.71
0.82
0.86
0.54
0.51
0.82

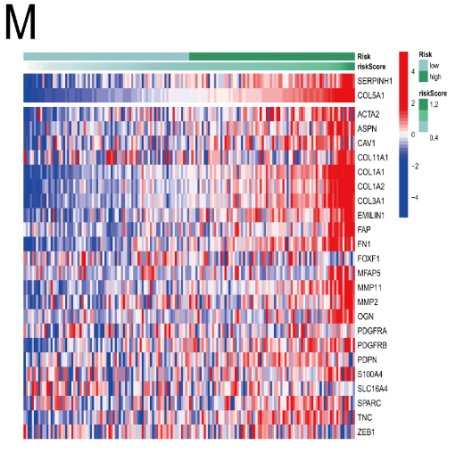
M
Risk
riskScore
SERPINH1
COL5A1
ACTA2
ASPN
CAV1
COL11A1
COL1A1
COL1A2
COL3A1
EMILIN1
FAP
FN1
FOXF1
MFAP5
MMP11
MMP2
OGN
PDGFRA
PDGFRB
PDPN
S100A4
SLC16A4
SPARC
TNC
ZEB1

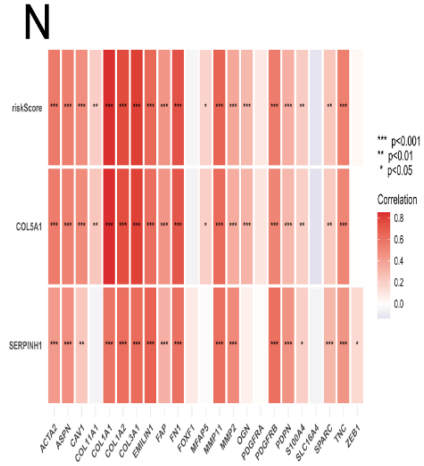
N
riskScore
COL5A1
SERPINH1
*** p<0.001
** p<0.01
* p<0.05
Correlation
ACTA2 ASPN CAV1 COL11A1 COL1A1 COL1A2 COL3A1 EMILIN1 FAP FN1 FOXF1 MFAP5 MMP11 MMP2 OGN PDGFRA PDGFRB PDPN S100A4 SLC16A4 SPARC TNC ZEB1

Figure 1. Construction of CAF prognostic model, and gene screening and validation. (A, B) Survival curves for TCGA (A) and GEO (B) data obtained using the four CAF-scoring algorithms. **(C, D)** Weighted correlation network analysis (WGCNA) of TCGA (C) and GEO data (D). Horizontal coordinates are the scored items, and vertical coordinates are the module names. Red color represents positive correlation, and blue represents negative correlation. The correlation coefficient is shown at the top of the module, and the p-value used for correlation assessment is shown at the bottom. $p < 0.05$ is correlated with CAFs expression levels. **(E)** Intersection genes in TCGA and GEO datasets. **(F)** Univariate Cox regression analysis. Red indicates high risk. **(G, H)** Lasso Cox regression analysis (lasso Lambda and lasso Cvfit). **(I)** Kaplan–Meier curves for the survival analysis of the high- and low-risk groups in TCGA and GEO datasets, respectively. **(J, K)** Prognostic analyses of SERPINH1 (J) and COL5A1 (K) using mRNA data from the Chinese Glioma Genome Atlas (CGGA). **(L)** Correlation between CAF scores and patient risk scores. Correlation coefficient is shown at the top right. Scatter plot of correlations is shown in the lower left quadrant of the figure. The diagonal sequence of squares represents the type of scoring algorithm. The last column represents the correlation between the CAF scores and patient scores. **(M)** Heat map of two identified CAF-related genes and CAF genes reported in the literature. **(N)** Correlation analysis of CAF genes reported in the literature, the two identified CAF-related genes, and risk scores.

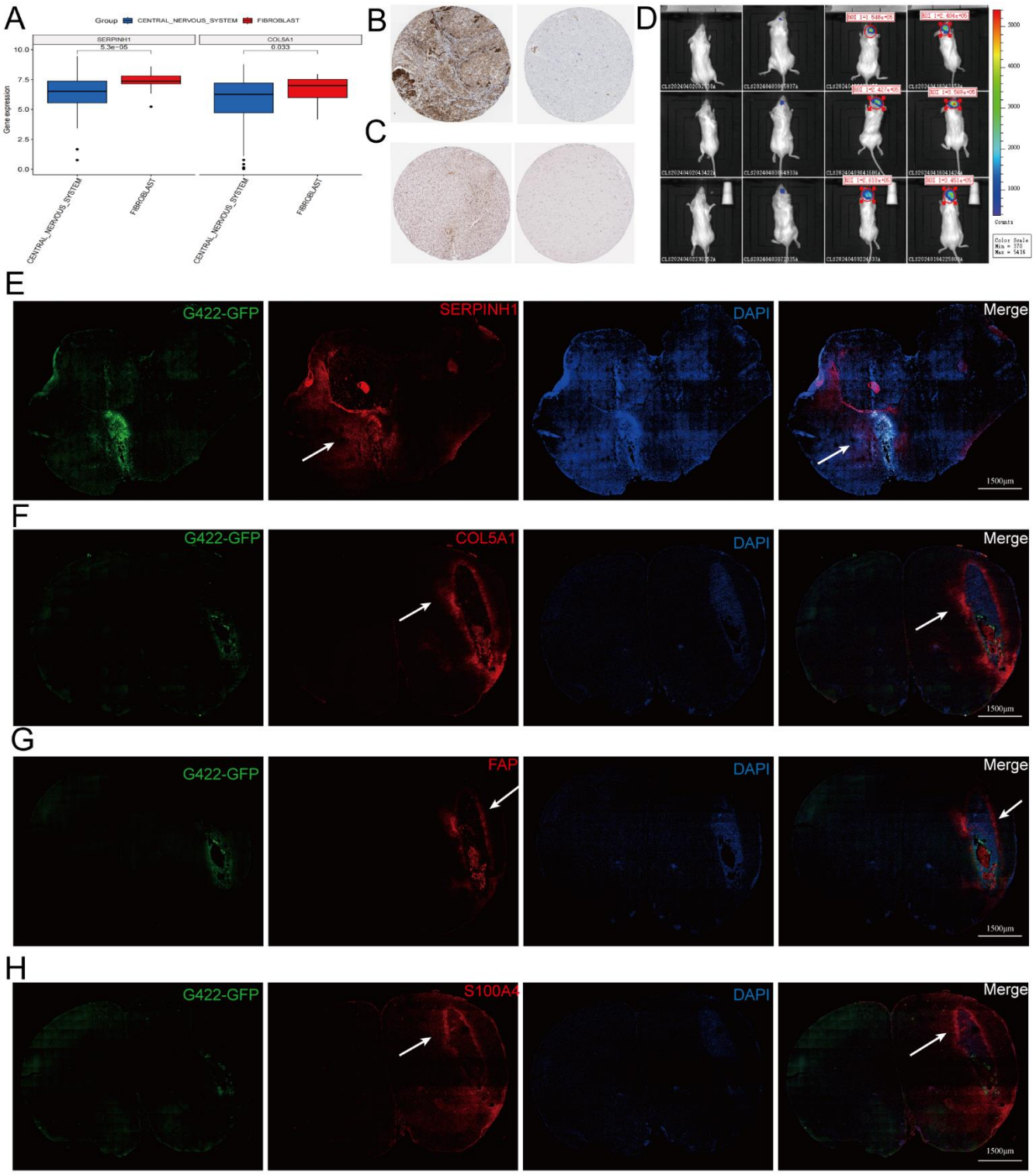
A
Group CENTRAL_NERVOUS_SYSTEM FIBROBLAST
SERPINH1
COL5A1
5.3e−05
0.033
Gene expression
CENTRAL_NERVOUS_SYSTEM
FIBROBLAST
B
C
D
E
G422-GFP
SERPINH1
DAPI
Merge
1500μm
F
G422-GFP
COL5A1
DAPI
Merge
1500μm
G
G422-GFP
FAP
DAPI
Merge
1500μm
H
G422-GFP
S100A4
DAPI
Merge
1500μm

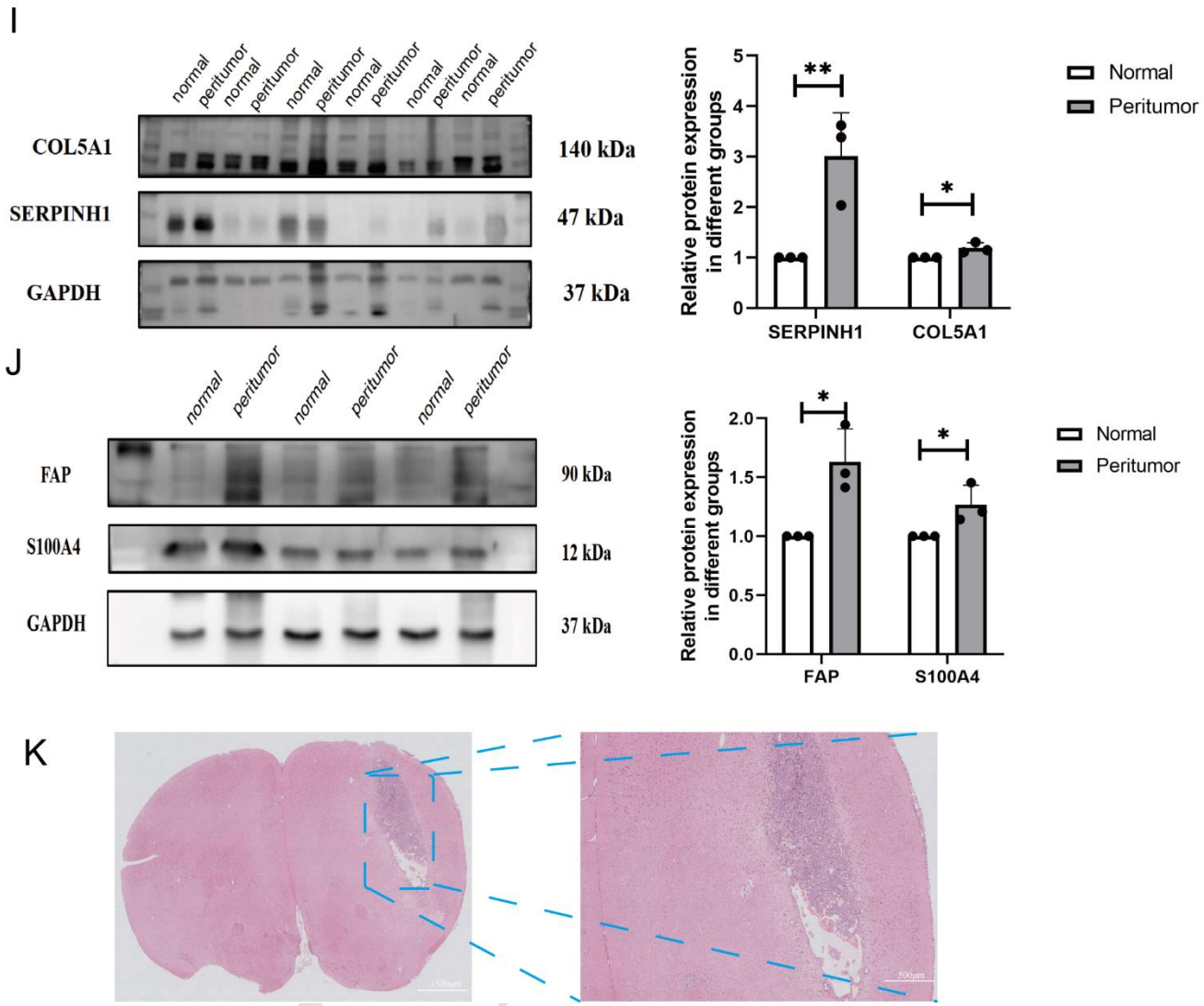

Figure 2. Detection, localization, and expression of SERPINH1 and COL5A1. **(A)**Expression of SERPINH1/COL5A1 in central nervous system (CNS) tumors and fibroblasts from the Cancer Cell Line Encyclopedia (CCLE) database. **(B, C)** Immunolabeling of SERPINH1 (B) and COL5A1 (C) in the GBM (left) and normal tissue (right) from the HPA database. **(D)** Tumor volumes were analyzed using bioluminescence imaging. **(E-H)** Multicolor IHC labeling of SERPINH1 (E), COL5A1 (F), FAP (G), and S100A4 (H) expression in the GBM mouse model. Green indicates G422-GFP expression. Red indicates the four CAF-associated proteins (SERPINH1, COL5A1, FAP, S100A4). Nuclei were stained using DAPI. Merge panel shows the combined image. White arrow indicates peritumor tissues with high expression of the indicated protein. **(I-J)** Western blotting analysis of the four CAF proteins in peritumor and normal tissues (FAP, 1.632 ± 0.279, n = 3; S100A4, 1.269 ± 0.165, n = 3; SERPINH1, 3.014 ±0.855, n = 3; COL5A1, 1.188 ±0.104, n = 3). **(K)** HE staining in the brain tissues of GBM mice. The experiment was

repeated three times, and the results are representative of three independent experiments. The statistical results are shown in Figure S7.

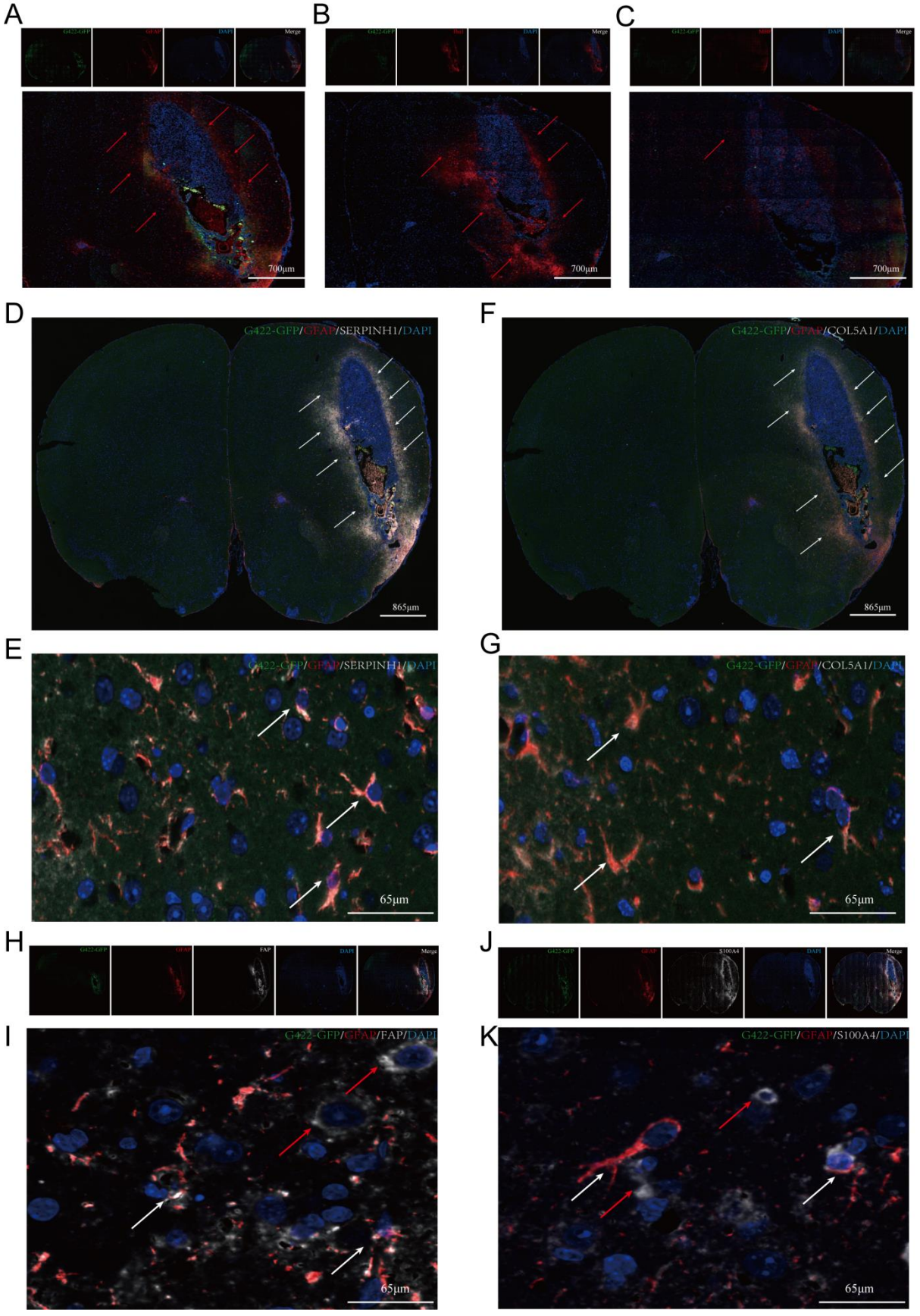

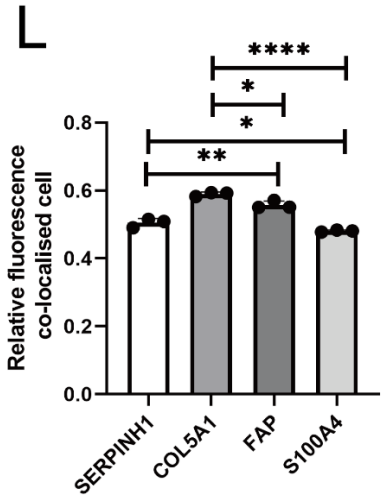

Figure 3. Localization of SERPINH1 and COL5A1. (A-C) Multicolor IHC staining of astrocytes (A, gfap), microglia (B, Iba1), and oligodendrocytes (C, MBP) in the GBM mouse model. Green indicates G422-GFP and Red indicates glial cells. Nuclei were stained using DAPI. The Merge panel shows the combined image. Red arrows indicate the localized recruitment of glial cells. The statistical results are shown in Figure S7. **(D-G)** Co-localization labeling of SERPINH1 (D, 10×; E, 63×) and COL5A1 (F, 10×; G, 63×) with astrocytes in the GBM mouse model. Green indicates G422-GFP, and Red indicates astrocytes. White indicates SERPINH1/COL5A1 expression. Nuclei were stained using DAPI. The Merge panel shows the combined image. White arrows indicate areas with high levels of co-localization and the cells that co-localized. **(H-K)** Co-localization labeling of FAP (H, 10×; I, 63×) and S100A4 (J, 10×; K, 63×) with astrocytes in the GBM mouse model. Green indicates G422-GFP, and Red indicates astrocytes. White indicates FAP/S100A4 expression. Nuclei were stained using DAPI. The Merge panel shows the combined image. White arrows indicate areas with high levels of co-localization and the cells that co-localized. Red arrows indicate FAP/S100A4-positive and GFAP-negative cells. **(L)** Statistical chart of tissue immunofluorescence localization (E, G, I, K) results SERPINH1,0.557 ± 0.011, n = 3; COL5A1, 0.590 ± 0.006, n = 3; FAP, 0.505 ± 0.013, n = 3; S100A4, 0.481 ± 0.003, n = 3. The experiment was repeated three times, and the results are representative of three independent experiments. In the statistical figures, p-values are indicated with asterisks, where * represents $p < 0.05$, ** represents $p < 0.01$, *** represents $p < 0.001$, and **** represents $p < 0.0001$.

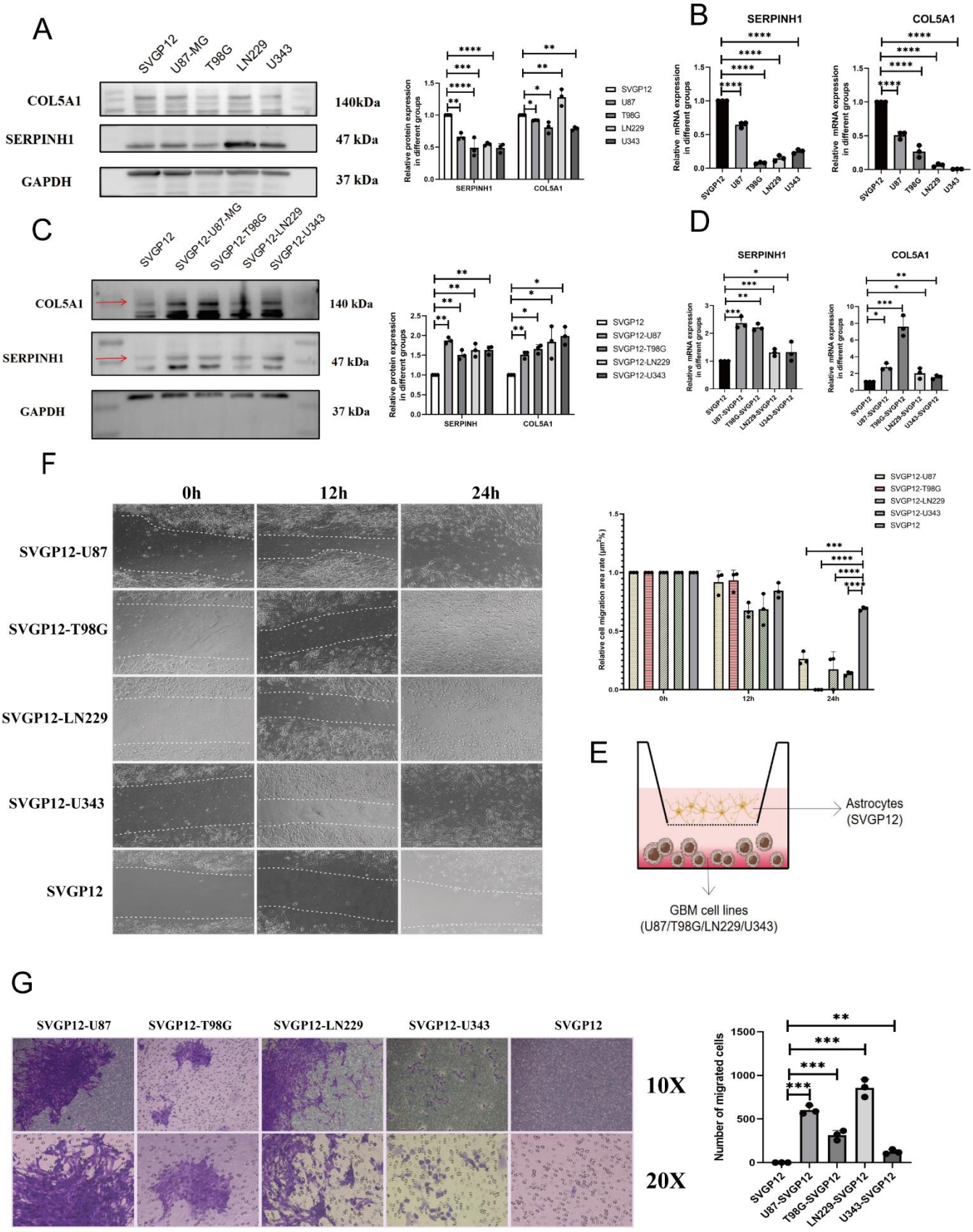

Figure 4. The expression of SERPINH1 /COL5A1 and cell function assays in a GBM-astrocytes co-culture model. (A, B) Western blotting (A) (SERPINH1: SVGP12, 1 ± 0, n =

3; U87, 0.664 ± 0.054, n = 3; T98G, 0.490 ± 0.146, n = 3; LN229, 0.547 ± 0.023, n = 3; U343, 0.487 ± 0.067, n = 3. COL5A1: SVGP12, 1 ± 0, n = 3; U87, 0.819 ± 0.169, n = 3; T98G, 0.809 ± 0.089, n = 3; LN229, 1.280 ± 0.130, n = 3; U343, 0.789 ± 0.026, n = 3.) and RT-qPCR (B) (SERPINH1: SVGP12, 1 ± 0, n = 3; U87, 0.646 ± 0.041, n = 3; T98G, 0.077 ± 0.012, n = 3; LN229, 0.147 ± 0.042, n = 3; U343, 0.250 ± 0.029, n = 3.COL5A1: SVGP12, 1 ± 0, n = 3; U87, 0.509 ± 0.054, n = 3; T98G, 0.268 ± 0.089, n = 3; LN229, 0.065 ± 0.023, n = 3; U343, 0.007 ± 0.002, n = 3.) in SVGP12 and GBM cell lines. **(C, D)** Western blotting (C)（SERPINH1: SVGP12, 1 ± 0, n = 3; SVGP12-U87, 1.871 ± 0.077, n = 3; SVGP12-T98G, 1.509 ± 0.117, n = 3; SVGP12-LN229, 1.628 ± 0.166, n = 3; SVGP12-U343, 1.635 ± 0.106, n = 3.COL5A1: SVGP12, 1 ± 0, n = 3; SVGP12-U87, 1.514 ± 0.088, n = 3; SVGP12-T98G, 1.659 ± 0.108, n = 3; SVGP12-LN229, 1.836 ± 0.410, n = 3; SVGP12-U343, 1.990 ± 0.228, n = 3.） and RT-qPCR (D) (SERPINH1: SVGP12, 1 ± 0, n = 3; SVGP12-U87, 2.367 ± 0.217, n = 3; SVGP12-T98G, 2.211 ± 0.125, n = 3; SVGP12-LN229, 1.308 ± 0.128, n = 3; SVGP12-U343, 1.324 ± 0.348, n = 3.COL5A1: SVGP12, 1 ± 0, n = 3; SVGP12-U87, 2.759 ± 0.425, n = 3; SVGP12-T98G, 7.595 ± 1.252, n = 3; SVGP12-LN229, 2.027 ± 0.629, n = 3; SVGP12-U343, 1.561 ± 0.246, n = 3.) in a co-culture model. **(E)** Schematic diagram of GBM-astrocytes in co-culture. **(F)** Wound healing assay in co-cultured SVGP12 (24h: SVGP12, 0.692 ± 0.016, n = 3; U87, 0.264 ± 0.051, n = 3; T98G, 0 ± 0, n = 3; LN229, 0.174 ± 0.151, n = 3; U343, 0.137 ± 0.017, n = 3.). **(G)** Migration assay in co-cultured SVGP12.(SVGP12, 1 ± 1, n = 3; U87, 603 ± 49.96, n = 3; T98G, 314 ± 55.05, n = 3; LN229, 856.7 ± 100.3, n = 3; U343,124.0 ± 26.21, n = 3). The statistical results are shown in Figure S7. The experiment was repeated three times, and the results are representative of three independent experiments. In the statistical figures, p-values are indicated with asterisks, where * represents $p < 0.05$, ** represents $p < 0.01$, *** represents $p < 0.001$, and **** represents $p < 0.0001$.

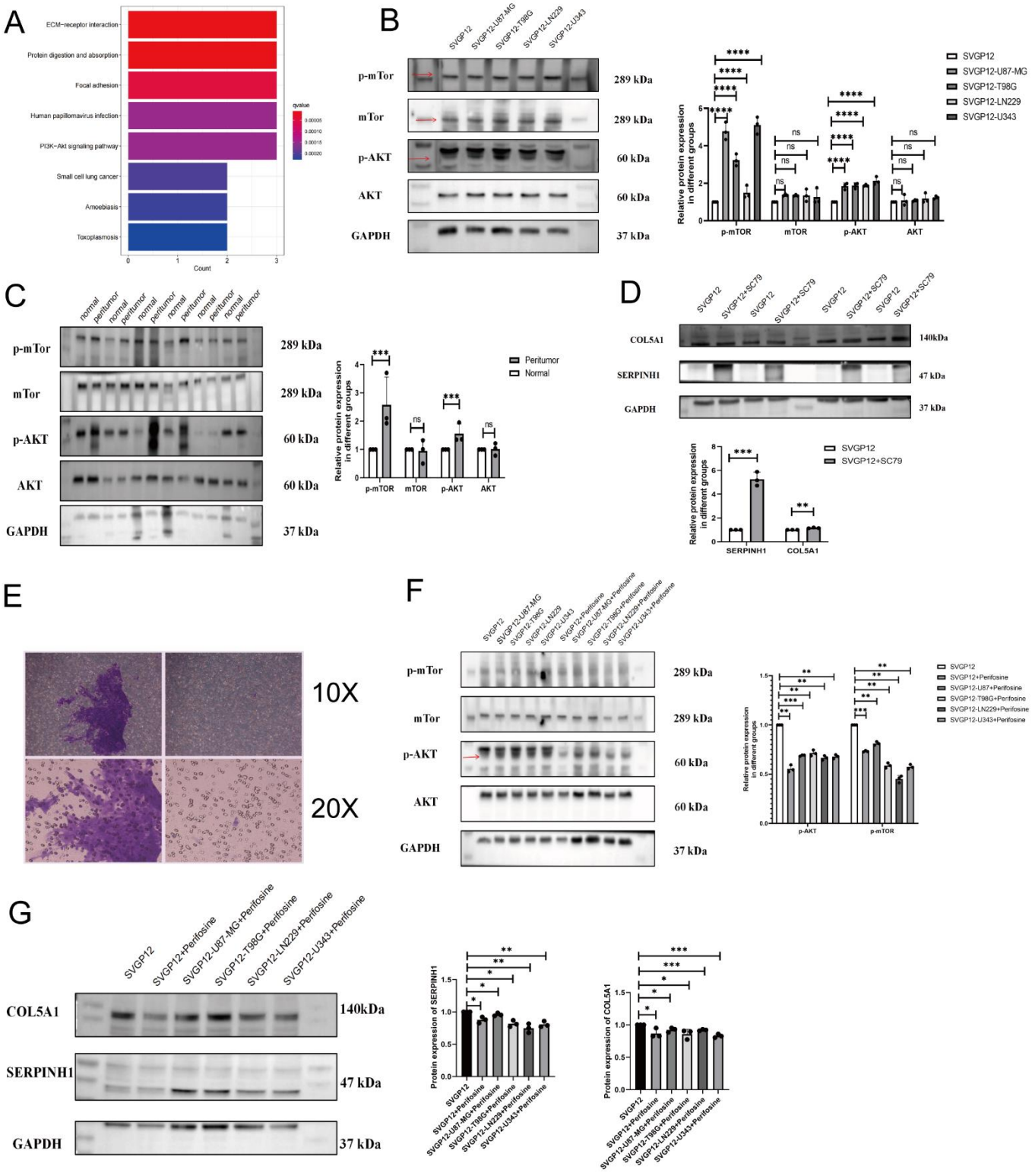

Figure 5. The expression of SERPINH1/ COL5A1 and AKT/m-TOR pathway in a GBM and astrocytes co-culture model. (A) KEGG pathway enrichment. **(B)** Western blot shows the expression of the AKT/m-TOR pathway in co-cultured SVGP12 cells (p-mTOR: SVGP12, 1 ± 0, n = 3; SVGP12-U87, 4.776 ± 0.467, n = 3; SVGP12-T98G, 3.234 ± 0.316, n

= 3; SVGP12-LN229, 1.497 ± 0.349, n = 3; SVGP12-U343, 5.107 ± 0.456, n = 3.mTOR: SVGP12, 1 ± 0, n = 3; SVGP12-U87,1.367 ± 0.054, n = 3; SVGP12-T98G, 1.349 ± 0.043, n = 3; SVGP12-LN229, 1.350 ± 0.330, n = 3; SVGP12-U343, 1.261 ± 0.438, n = 3. p-AKT: SVGP12, 1 ± 0, n = 3; SVGP12-U87, 1.847 ± 0.168, n = 3; SVGP12-T98G, 1.880 ± 0.152, n = 3; SVGP12-LN229, 1.877 ± 0.053, n = 3; SVGP12-U343, 2.127 ± 0.213, n = 3.AKT: SVGP12, 1 ± 0, n = 3; SVGP12-U87, 1.089 ± 0.287, n = 3; SVGP12-T98G, 1.075 ± 0.044, n = 3; SVGP12-LN229, 1.183 ± 0.269, n = 3; SVGP12-U343, 1.237 ± 0.077, n = 3). **(C)** Western blot shows AKT/m-TOR pathway expression in peritumor and normal tissues of GBM mice (p-mTOR: Normal, 1 ± 0, n = 3; Peritumor, 2.578 ± 0.981, n = 3. mTOR: Normal, 1 ± 0, n = 3; Peritumor,0.944 ± 0.413, n = 3. p-AKT: Normal, 1 ± 0, n = 3; Peritumor, 1.554 ± 0.349, n = 3. AKT: Normal, 1 ± 0, n = 3; Peritumor, 1.011 ± 0.218, n = 3). **(D)** Western blot shows SERPINH1 and COL5A1 expression in SVGP12 cells treated with the AKT agonist sc79 (SERPINH1:SVGP12, 1 ± 0, n = 3; SVGP12+SC79, 5.263 ± 0.584, n = 3. COL5A1:SVGP12, 1 ± 0, n = 3; SVGP12+SC79, 1.160 ± 0.033, n = 3). **(E)** Migration of SVGP12 cells treated with the AKT agonist sc79 (right) and of untreated SVGP12 cells (left). **(F, G)** Western blot shows the expression of the AKT-mTOR pathway (F) (p-mTOR: SVGP12, 1 ± 0, n = 3; SVGP12+Perifosine, 0.782 ± 0.007, n = 3; SVGP12-U87+Perifosine, 0.812 ± 0.018, n = 3; SVGP12-T98G+Perifosine, 0.588 ± 0.026, n = 3; SVGP12-LN229+Perifosine, 0.451 ± 0.035, n = 3; SVGP12-U343+Perifosine, 0.574 ± 0.023, n = 3. p-AKT: SVGP12, 1 ± 0, n = 3; SVGP12+Perifosine, 0.555 ± 0.036, n = 3; SVGP12-U87+Perifosine, 0.690 ± 0.006, n = 3; SVGP12-T98G+Perifosine, 0.714 ± 0.030, n = 3; SVGP12-LN229+Perifosine, 0.665 ± 0.023, n = 3; SVGP12-U343+Perifosine, 0.677 ± 0.021, n = 3.) and that of SERPINH1 and COL5A1 (G) in co-cultured SVGP12 cells, and in co-cultured SVGP12 cells treated with the AKT inhibitor perifosine (SERPINH1: SVGP12, 1 ± 0, n = 3; SVGP12+Perifosine, 0.876 ± 0.048, n = 3; SVGP12-U87+Perifosine, 0.959 ± 0.023, n = 3; SVGP12-T98G+Perifosine, 0.817 ± 0.050, n = 3; SVGP12-LN229+Perifosine, 0.748 ± 0.070, n = 3; SVGP12-U343+Perifosine, 0.807 ± 0.046, n = 3.COL5A1:SVGP12, 1 ± 0, n = 3; SVGP12+Perifosine, 0.868 ± 0.072, n = 3; SVGP12-U87+Perifosine, 0.923 ± 0.034, n = 3; SVGP12-T98G+Perifosine, 0.859 ± 0.074, n = 3; SVGP12-LN229+Perifosine, 0.920 ± 0.011, n = 3; SVGP12-U343+Perifosine, 0.830 ± 0.028, n = 3). **(H)** Statistical graph of changes in SERPINH1 and COL5A1 protein expression with the addition of perifosine. The experiment was repeated three times, and the results are representative of three independent experiments. The statistical results are shown in Figure S7. In the statistical figures, p-values are indicated

with asterisks, where * represents $p < 0.05$, ** represents $p < 0.01$, *** represents $p < 0.001$, and **** represents $p < 0.0001$.

SUPPLEMENTAL DATA

Table S1. Sequences of primers used in this research

Targets	Forword5'-3'	Revers5'-3'
SERPINH1	TGCTAGTCAACGCCATGTTCT	ATAGGACCGAGTCACCATGAA
COL5A1	TACCCTGCGTCTGCATTTCC	GCTCGTTGTAGATGGAGACCA
β-actin	AAGATCATTGCTCCTCCTG	CATACTCCTGCTTGCTGAT